Chem Soc Rev

TUTORIAL REVIEW

View Article Online
View Journal | View Issue

Cite this: *Chem. Soc. Rev.*, 2023, 52, 6344

Strategies to convert organic fluorophores into red/near-infrared emitting analogues and their utilization in bioimaging probes

Mingchong Dai, *[ab] Yun Jae Yang,[a] Sourav Sarkar[a] and Kyo Han Ahn *[a]

Received 12th July 2023

DOI: 10.1039/d3cs00475a

rsc.li/chem-soc-rev

Organic fluorophores aided by current microscopy imaging modalities are essential for studying biological systems. Recently, red/near-infrared emitting fluorophores have attracted great research efforts, as they enable bioimaging applications with reduced autofluorescence interference and light scattering, two significant obstacles for deep-tissue imaging, as well as reduced photodamage and photobleaching. Herein, we analyzed the current strategies to convert key organic fluorophores bearing xanthene, coumarin, and naphthalene cores into longer wavelength-emitting derivatives by focussing on their effectiveness and limitations. Together, we introduced typical examples of how such fluorophores can be used to develop molecular probes for biological analytes, along with key sensing features. Finally, we listed several critical issues to be considered in developing new fluorophores.

Key learning points

1. Importance of red/NIR emitting fluorophores.
2. Feasibility and challenges to convert conventional fluorophores into their red/NIR emitting analogues.
3. Molecular-level understanding of the correlation between the structural modifications and the bathochromic emission shifts.
4. Bio-relevant applications (utilization in bioimaging probes) of red/NIR emitting fluorophores.
5. Scope and limitations of conventional structural modification methods.

1. Introduction

Organic fluorophores are essential for bioimaging applications due to their distinctive characteristics, such as non-invasiveness, high sensitivity and selectivity, and capability for real-time imaging. Such advantages also hold immense promise for clinical applications.[1] Fluorophores emitting in the longer wavelengths, preferably in the red/near-infrared (NIR) region, are in great demand for bioimaging of tissues with reduced autofluorescence interference and at deeper imaging depths. The issue of autofluorescence, arising from innate biomolecules, presents a significant concern in tissue imaging at deeper depths. Due to the emission of fluorescent biomolecules, including NAD(P)H, flavins, lipofuscin, *etc.*, mostly in the blue, green, and orange wavelengths,[2] utilizing fluorophores that emit in the red (>630 nm) or near-infrared (NIR) region is essential for bioimaging applications (Fig. 1a–d). Failing to do so could lead to substantial autofluorescence interference in tissue imaging.[3] The magnitude of autofluorescence varies across different tissue types, exhibiting notable levels in the green and yellow emission channels but diminishing beyond approximately 630 nm (Fig. 1e–g).[4] Additionally, the excitation of fluorophores at longer wavelengths leads to reduced photo-bleaching of them and reduced photo-damaging of biological samples. Accordingly, great efforts have been made to develop longer-emitting dyes from typical organic fluorophores, leading to significant progress in this field.[5] Hence, it is crucial to prioritize the development of fluorophores with emissions in the red/NIR region. At this point, it is worth noting that currently there is no consensus on using the terminology "NIR" among scientists working in the field of fluorescent probes. A dye is frequently claimed to be a NIR dye when its emission spectra cover some portion above 700 nm or so, even though the maximum is below 700 nm. The "red" wavelength

[a] *Department of Chemistry, Pohang University of Science and Technology, Pohang, 37673, South Korea. E-mail: daimingchong@postech.ac.kr, ahn@postech.ac.kr*
[b] *CEDAR, Knight Cancer Institute, School of Medicine, Oregon Health & Science University, Portland, Oregon, 97201, USA. E-mail: daimin@ohsu.edu*

region ranges from 620 to 750 nm and that for the NIR from 700 to 1500 nm (according to the IEC 60050-845:2007 standard), generating an overlapping region between red and NIR, from 700 to 750 nm. It may be acceptable to claim a NIR dye if its emission maximum is above 700 nm.

In this tutorial review, we wish to introduce key strategies that convert several common organic fluorophores into analogues that emit in longer wavelengths, preferably in the red/NIR wavelength region. Commonly used strategies involve π-conjugation extension, modification of the electron-donor and -acceptor groups, and replacement of the central heteroatom in xanthene dyes, which can be best demonstrated with the fluorophores based on xanthene, coumarin, and naphthalene cores. Organic fluorophores having xanthene, coumarin, and naphthalene cores can be readily functionalized and thus have been widely used for biological applications. These fluorophores also provide good starting points for the development of longer-emitting derivatives. The structural modifications lead to variable emission bathochromic shifts, which are also dependent on the molecular geometry. Understanding the ''effective'' directions for the structural modifications toward the bathochromic emission spectral shift will provide valuable design guidance to new organic fluorophores with desirable features for bioimaging applications. Herein we analyzed the key structural modifications of the fluorophores for the bathochromic shift categorized by the core structures. Besides, we briefly introduced how these fluorophores can find their applications in studying biological issues.

Mingchong Dai

Dr Mingchong Dai received his BS from the South-Central University for Nationalities in 2012 and his MS from Hunan University in 2015. Later, he joined Prof. Kyo Han Ahn's group at POSTECH and earned his PhD in 2020. He was a postdoctoral scholar at POSTECH until 2022. Currently, he is a postdoctoral scholar at Cancer Early Detection Advanced Research Center, OHSU Knight Cancer Institute, his research is focused on fluorophore chemistry, molecular probes in early cancer fluorescence-related technology, detection, etc.

Yun Jae Yang

Yun Jae Yang was born and raised in the Republic of Korea. She received her BS degree in Chemistry from the Sookmyung Women's University. She is now a 5th year PhD student working with Prof. Kyo Han Ahn at POSTECH, South Korea. Her research interest includes fluorescent organic molecular probes and their bioimaging applications.

Sourav Sarkar

Dr Sourav Sarkar received his BS from the University of Calcutta in 2013 and MS from IIT Kharagpur in 2015. Later, he joined Prof. Kyo Han Ahn's group at POSTECH and earned his PhD in 2020. He was appointed as a research assistant professor at POSTECH in 2022. His research is focused on molecular probes, environment-insensitive fluorophores, redox biology, organelle dynamics etc.

Kyo Han Ahn

Dr Kyo Han Ahn currently holds the title of Specially Designated/Emeritus Professor at POSTECH. His educational journey includes the attainment of a BS degree from Seoul National University in 1980 and a PhD degree in Organic Chemistry from KAIST in 1985. His research efforts garnered him several distinguished awards, including the Oder of Science and Technological Merit bestowed by the Republic of Korea, along with the Academic Excellence Prize granted by the Korean Chemical Society. He holds the title of Fellow of the Korean Academy of Science and Technology. Professor Ahn's research journey has traversed diverse terrains, initially encompassing organic synthesis and organometallic catalysts, and subsequently expanding into the realms of molecular recognition, luminescent materials, and molecular probes for bioimaging.

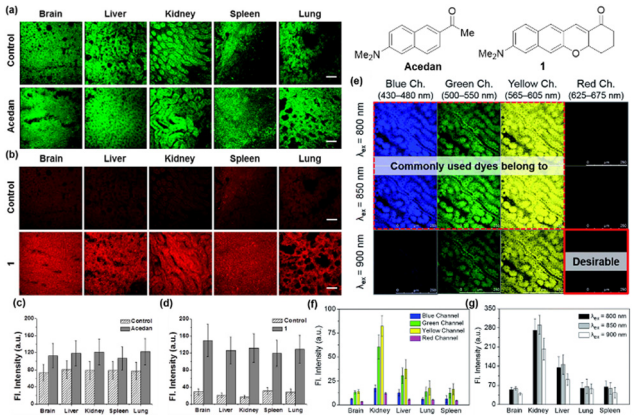

Fig. 1 Fluorescent images of mouse tissues (brain, liver, kidneys, spleen, and lungs from the left) stained with (a) acedan (10 μM) and (b) its π-extended analogue, observed under two-photon excitation at 780 and 900 nm, respectively. (c) and (d) Relative fluorescence intensities of the images of (a) and (b), respectively. (e) Autofluorescence images of mouse kidney tissues, obtained under two-photon excitation at 800, 850, and 900 nm, and emission collection through blue (430–480 nm), green (500–550 nm), yellow (565–605 nm), and red (625–675 nm) channels. (f) Comparison of the total autofluorescence intensities from the four emission channels between different organ tissues (brain, kidneys, liver, lungs, and spleen); (g) comparison of the total autofluorescence intensities between the organ tissues depending on the excitation wavelength. Reproduced permission: (a)–(d) Copyright©2015, American Chemical Society. (e)–(g) Licensed under a Creative Commons Attribution-Non Commercial 3.0 Unported Licence.

2. Xanthene derivatives

The widely used rhodamine and fluorescein dyes are xanthene (10*H*-9-oxa-anthracene) derivatives with nitrogen and oxygen substitutions both at C-2 and C-7, respectively, together with the (*o*-carboxy)phenyl substituent at C-9. Rhodamine and fluorescein analogues simply with a phenyl substituent at C-9 are called rosamine and fluorone dyes, respectively (here denoted as CFPX). A hybrid form between rhodamine and fluorescein is named rhodol, and that between rosamine and fluorone is named rosol (Fig. 2a). Among them, the carboxyphenyl-containing dyes can exist in their spiro-lactone forms in equilibration with the ring-opened zwitterionic forms. The spiro-lactone ring-opening and -closing conversion process offers fluorescence on–off signalling in the fluorescence sensing of biological systems (Fig. 2b).[6] The photophysical properties, particularly, the emission wavelengths, of the xanthene dyes are affected by: (a) the amino substituent (in red, Fig. 2c), (2) the C-9 central atom (in orange, Fig. 2c), and (3) the conjugation length (in blue, Fig. 2c).

2.1. *o*-Carboxyphenyl-substituted xanthene dyes

2.1.1. The amino group effect. The alkyl amines of the push–pull type fluorophores act as electron-donating groups in conjugation with their iminium forms, which significantly affect the emission properties of the fluorophore.[4] When going from rhodamine 123 (–NH_2) to rhodamine 6G (–NHEt) and rhodamine B (–NEt_2), the emission maximum shows bathochromic shifts from 532 nm to 553 nm and 576 nm (in ethanol), respectively. The emission wavelengths of the dialkylamine-substituted rhodamines (rhodamines B, rhodamine 101, and rhodamine 630) are in the order: diethylamine (576 nm) < julolidine (595 nm) < ethyl-indoline (616 nm) (Fig. 3). From the results, it is concluded that a better electron-donating amino group is preferred for the bathochromic emission shift of such rhodamine dyes. However, the maximum emission wavelengths of those "monoamine-substituted" rhodamines are still not reached in the deep-red region by modifying the monoamine substituent alone. Zhang and co-workers disclosed that using xanthene dyes with "diamino" substituents, instead of the mono-amino donors, is an effective way to induce significant bathochromic shifts in their absorption and emission maxima, as demonstrated with new deep-red/NIR emitting pyronine and silapyronine analogues.[8–10]

2.1.2. Central atom replacement. The C-9 central atom of the xanthene dyes can be chosen from the carbon family (group 14: C, Si, Ge, and Sn), leading to various xanthene analogues,[11–23] as well as from the nitrogen family (group 15; N and P)[16,24] or chalcogen family (group 16; O, S, Se, and Te)[16,25–28] (Fig. 4). The replacement of the central oxygen atom in the xanthene dyes leads to variable bathochromic emission shifts, and the underlying mechanisms are also different. For the atoms of groups 14 and 15, it was explained that the X atom (Si, Ge, Sn, and P) can stabilize the LUMO energy levels by the σ*–π* conjugation between the σ* orbitals of the exocyclic X–C

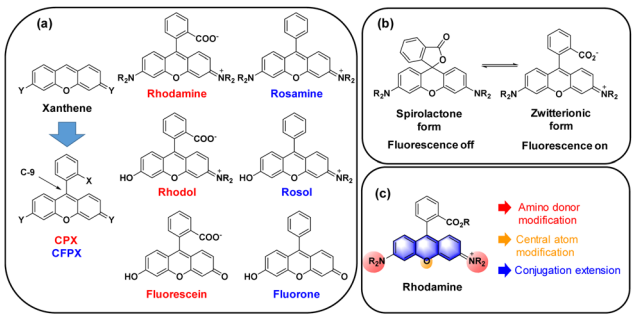

Fig. 2 (a) Structures of C-9 phenyl-substituted xanthene dyes. (b) Spiro-lactone and zwitterionic forms of rhodamines. (c) Modifications to extend the emission wavelengths of rhodamines.

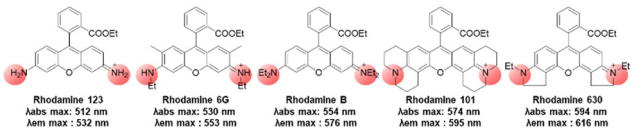

Fig. 3 The effect of the amino group on the absorption and emission wavelengths of rhodamine dyes,[7] observed in ethanol.

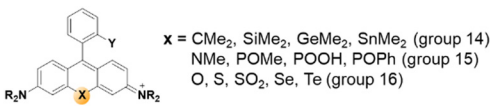

Fig. 4 Candidate elements/groups for the replacement of central atom X.

or X═O bond (for example, –SiMe$_2$, –P(═O)OH, –P(═O)Me, and –P(═O)Ph) and the π* orbital of the fluorophore nearby.[29,30] For the atoms of group 16, the heteroatom lone pair occupancy and resonance stability are found to be the major determinants of the excitation energetics: the X atom of S, Se, or Te showed increased lone pair occupancy, which lowers the excitation energy and thus leads to longer absorption wavelengths.[27]

A systematic variation of the central oxygen atom of rhodamines has been conducted by Lavis and co-workers.[16] The maximum absorption and emission wavelengths of rhodamine analogues with amine (nitrogen), sulfur, sulfone, carbon, silicon, phosphinate, or phosphine oxide at the central C-9 are listed in Fig. 5. By the substitution of the central atom, the bathochromic emission wavelength shift increased in the order of N, O, S, C, Si, and P. Together with the known red-shift effect by the azetidine group, the maximum emission wavelength of 723 nm (pH 7.3 HEPES buffer) was realized with the –P(═O)Ph analogue. Note that the replacement of the C-9 oxygen atom with silyl (–SiR$_2$) groups to obtain deep-red/NIR-emitting dyes has received much attention, plausibly owing to the synthetic feasibility. The replacement of the C-9 oxygen atom with the dimethylsilyl group, for example, leads to increased electrophilicity at C-10. Accordingly, the spiro-lactone ring-opening takes place in media of rather higher polarities compared to the case of the corresponding rhodamine analogues. Recently, a rosamine analogue with a boron substituent at C-9 (B-(OH$_2$)) was also reported; the rosamine borinic acid emits at around 650 nm.[31]

2.1.3. π-Conjugation extension. The extension of the π-conjugation length of a fluorophore is a common way to shift its absorption/emission maxima. Herein, rhodamine derivatives with a fused benzene ring, called benzorhodamine dyes, are discussed. Depending on the site of ring fusion, they can be categorized into linear- and bent-shape benzorhodamine dyes.

Up to now, four types of geometrically different benzorhodamines have been reported: benzorhodamine **a-I**,[32] **b-II**,[33] **c-I**[34] and **c-II**[35] types. These benzorhodamines showed significantly red-shifted emission wavelengths at more than 635 nm, reaching 785 nm in the case of linear **b-II**. Recently, Liu and co-workers disclosed a novel π-extension approach based on computational calculations, which led to dual-emission rhodamine analogues from single-emission rhodamines. The π-extended rhodamines composed of selected fragments with matched FMO energy levels avoided the otherwise possible inter-fragment PeT.[36]

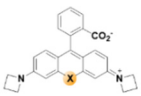

No	1	2	3	4	5	6	7	8
X								
λ_{abs} (nm)	502	549	570	608	646	668	704	n.d.
λ_{em} (nm)	533	571	593	631	664	687	723	n.d.

Fig. 5 Effect of the replacement of the central atom (X) on the maximum absorption/emission wavelengths of a rhodamine dye,[16] observed in HEPES at pH 7.3 (10 mM).

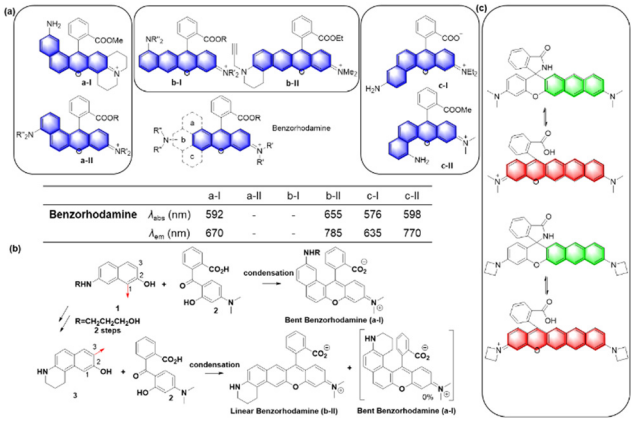

Benzorhodamine	a-I	a-II	b-I	b-II	c-I	c-II
λ_{abs} (nm)	592	-	-	655	576	598
λ_{em} (nm)	670	-	-	785	635	770

Fig. 6 (a) Structures of benzorhodamines. (b) Development of linear **b-II** type benzorhodamines. (c) Dual-emission π-extended rhodamines.

At this point, it is worthwhile to mention a synthetic challenge encountered in the context of linear benzocoumarin dyes (Fig. 6b). A condensation reaction of an amino-naphthol such as **1** with keto-benzoic acid **2** does not lead to the linear type but the **a-I** type bent benzorhodamine exclusively because the C-1 site of compound **1** is more nucleophilic than the C-3 site toward electrophiles. The regioselectivity issue was solved by introducing steric hindrance near the electrophilic C-1 site, leading to linear benzorhodamines.[33] Linearly conjugated dipolar dyes usually absorb and emit wavelengths longer than the corresponding bent analogues.[37]

2.1.4. CPX-based bioimaging probes, selected examples. The rhodamine and rhodol analogues can be developed into fluorescent probes, mostly activatable or reaction-based probes, by introducing reactive groups at the spiro-lactone or the N/O-donor groups, similar to the case of their parent dyes. The rhodamine spiro-lactam ring-opening process triggered by target analytes is an established strategy to realize fluorescence off–on signalling.[6] For example, rhodamine lactams **F1** and **F2** undergo the spirolactam ring-opening triggered by a reactive oxygen species, hypochlorous acid (**F1**, Fig. 7a),[38] and Cu^{2+}(**F2**, Fig. 7a),

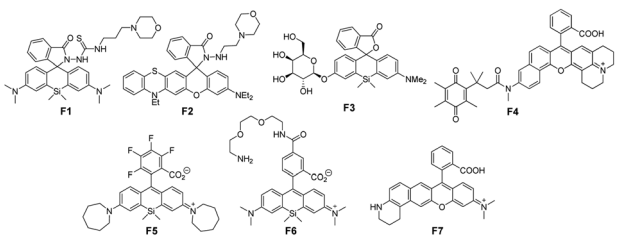

№	Abs/Em (nm)	Application	№	Abs/Em (nm)	Application
F1	PRD: $\lambda_{abs}/_{em}$: 660/680; PBS (pH 5)	HClO Sensing; HeLa, RAW276.7 cells; Mouse liver tissues; (Turn-On)	F5	PRB: $\lambda_{abs}/_{em}$: 683/698; HEPES (pH 7.3)	Membrane staining; U2OS, COS7 cells; (labeling)
F2	PRD: $\lambda_{abs}/_{em}$: 625/730; H_2O:MeCN=2:1	Cu^{2+} Sensing; HeLa, L929 cells; (Turn-On)	F6	PRB: $\lambda_{abs}/_{em}$: 649/666; PRD: $\lambda_{abs}/_{em}$: 649/662; HEPES (pH 7.4)	RNA imaging; *E. Coli* cells and bacteria; (labeling)
F3	PRD: $\lambda_{abs}/_{em}$: 610/638; PBS (pH 7.4)	β-galactosidase sensing; HEK-*lacZ* cells; Drosophila; Mouse tissue imaging (Brain); (Turn-On)	F7	PRB: $\lambda_{abs}/_{em}$: 632/755; PBS (pH 7.4, 30% EtOH)	Photothermal therapy; HeLa, HT29, A549, MDA-MB-231 cells; Mouse tissue imaging (Colon, heart, liver, lung); (labeling)
F4	PRD: $\lambda_{abs}/_{em}$: 585/624; PBS (pH 7.4)	hNQO1 or $S_2O_4^{2-}$ Sensing; HT29, H596 cells; (Turn-On)			

Fig. 7 Selected examples of fluorescent probes based on rhodamine and rhodol analogues.

respectively,[39] followed by hydrolysis to generate the corresponding fluorescent rhodamines. On the other hand, introducing a reactive group for the target analyte at the hydroxyl or amino (–OH or –NHR) donors in the rhodamine/rhodol/fluorescein dyes results in the corresponding nonfluorescent spiro-lactone forms, which, upon the treatment with target analytes, can regenerate the original fluorescent dyes. For example, the hydroxyl donor of the rhodol analogue protected with β-galactose reacts with β-galactosidase to generate the rhodol analogue. This process is accompanied by fluorescence off–on signalling.[20] Similarly, **F4** bearing a quinone substrate specific to human NAD(P)H quinone oxidoreductase-1 (hNQO1) undergoes enzyme-catalyzed reduction to give rise to hydroquinone, which triggers intramolecular cyclization followed by amide bond cleavage to regenerate the amino donor.[40] In this case, the quinone moiety can also act as a fluorescence quencher through photoinduced electron transfer (PeT); hence, the removal of the quinone moiety can cause the observed off–on fluorescence signal change.

The fluorophores can be also applied to the labelling of the cell membrane (**F5**, Fig. 7d)[19] and RNA (**F6**, Fig. 7d).[21] As the dyes are in the fluorescence-on state, washing-out steps are required in such applications.

Recently, Dai and co-workers have developed a synthetic route to obtain linear benzorhodamines. In the free carboxylic acid form such as **F7**, it absorbs light efficiently but emits weaker fluorescence compared to its ester form, which has the potential for photothermal therapy.[33] The linear benzorhodamine in the ester form is useful for NIR imaging.

2.2. Carboxy-free, phenyl-substituted xanthene fluorophores

2.2.1. Amino donor effect in rosols. Chin and co-workers reported that stronger electron-donating amino groups cause emission bathochromic shifts in rosol derivatives.[41] A similar trend was observed among the different amino donors in the case of rhodamine and rosamine dyes. In the case of the julolidine (a bicyclic amino donor) derivative Jul-Rosol, the emission maximum reached 574 nm, which is still away from deep-red wavelengths. Interestingly, a diamine-substituted analogue THQ-Rosol emits in the NIR region (λ_{em} = 710 nm) with a large bathochromic shift ($\Delta\lambda$ = 136 nm) from that of Jul-Rosol (Fig. 8), an important observation for the future development of NIR-emitting dyes.

2.2.2. Central X atom replacement. Both the rosol (Fig. 9a) and rosamine (Fig. 9b) systems show a similar level of spectral shifts to the case of rhodamines. Together with the data in Fig. 5, we can make rosol, rosamine, and rhodamine dyes emit in the deep-red or even in the NIR wavelength region by

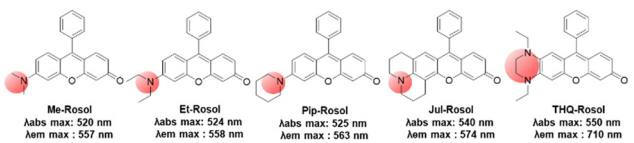

Fig. 8 The amino donor effect on the photophysical properties of rosol dyes.[41] The data were obtained in pH 7.4 phosphate buffer (50 mM, 150 mM NaCl).

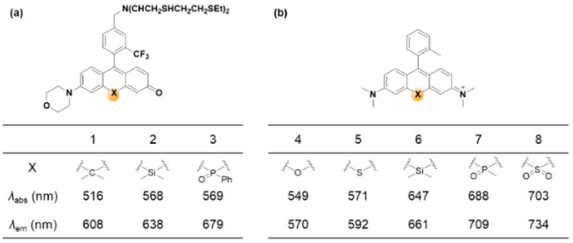

Fig. 9 Effects of central atom replacement on the photophysical properties of rosol (left) and rosamine (right). Data for dyes **1–3** are measured in HEPES buffer (25 mM, pH 7.4),[42] and those for dyes **4–8** are measured in PBS (20 mM, pH 7.4).[43]

replacing their central oxygen atom with Si, POPh, POOH, POMe, or SO_2.

As noted above, the replacement of the central oxygen atom of rhodamines with silyl groups affords the corresponding silarhodamine analogues (Si-rhodamines), which offer several advantageous features for bioimaging applications, such as deep-red emission[44] and enhanced two-photon (TP) properties.[45,46] Si-rhodamines have been also used for super-resolution imaging.[47] The replacement of the C-10 phenyl group of Si-rhodamines with an amine leads to the so-called amino-Si-pyronins that show unique optical properties. In contrast to the parent Si-rhodamines that show narrow Stokes shifts, amino-Si-pyronins exhibit large Stokes shifts. In addition, amino-Si-pyronins have excellent two-photon imaging capability, which is lacking in the case of Si-rhodamines. Si-rhodamines undergo a medium polarity-dependent spiro-lactone ring-opening and -closing equilibrium: they are highly fluorescent in the ring-opened form in highly polar media but nonfluorescent in the ring-closed form in nonpolar media. Amino-Si-pyronins can also exist in the fluorescence-on and -off states depending on the medium polarity. In highly polar media, amino-Si-pyronins are strongly fluorescent in the enamine form: contrarily, in nonpolar media, they are nonfluorescent in the imine form. This enamine–imine equilibrium is also dependent on the 2- and 7-amine substituents.[46] A promising aspect of amino-Si-pyronins is that we can further functionalize the C-10 amino group, such as *via* the introduction of an acyl or analogous group onto it. In this case, the electrophilicity of C-10 also increases; hence, biothiols such as cysteine can react with some acylated amino-Si-pyronins. This chemical stability issue can be solved by the julolidine-derived amino-Si-pyronins that are stable in cells. The resulting acyl analogues now emit in the NIR region, leading to a novel type of NIR dyes. Notably, amino-Si-pyronins and their NIR analogues constitute a novel sensing platform for the development of activity-based (activatable or reaction-based) probes. For example, two-photon ratiometric probes can be developed by introducing H_2O_2- or NTR-responsive moieties onto the C-10 amino group. In this case, the emission maxima change from a NIR to a deep-red region (hypochromic shift, Fig. 10b). Also, ratiometric sensing systems that show signal changes from the deep-red to NIR region (bathochromic shift, Fig. 10c) can be conceivable, as exemplified

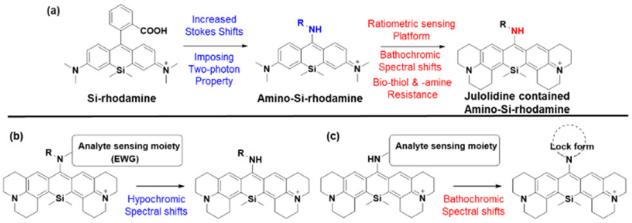

Fig. 10 (a) Development of chemically stable amino-Si-pyronins. Activatable sensing platforms based on the julolidine-derived amino-Si-pyronins for the ratiometric sensing of analytes with (b) bathochromic spectral shifts and (c) hypochromic spectral shifts.

by an HOCl probe (more examples are provided in the application section below).

2.2.3. Conjugation extension. Strongin and co-workers first developed all six types of benzofluorones (named **SNAFR**, Fig. 11a),[48] whose photophysical properties are altered similarly to the case of benzorhodamines. Among the benzofluorones, the **b-I** type has poor solubility and also shows marginal red-shifts. Other five types of benzofluorones emit in the red region (**a-I**, 653 nm; **c-I**, 629 nm) or even in the NIR region (**a-II**, 713 nm; **b-II**, 733 nm; **c-II**, 757 nm). Such benzene-fused dyes are expected to have enhanced photo- and chemo-stability compared to the highly π-conjugated dyes with vinyl units, such as cyanine and hemicyanine dyes, which can undergo addition and oxidation side reactions with highly nucleophilic or reactive oxygen species (HSO_3^-, HOCl, $ONOO^-$, *etc.*). Ahn and co-workers synthesized the linear-shaped benzene-fused rosol or rosamine analogues. The synthetic route, which is different from the case of rhodamines, required the triarylmethanol intermediate **3** (Fig. 11b), which, upon demethylation and intramolecular cyclization, afforded the desired benzorosol.[49,50] Furthermore, a free amine-containing benzorosamine, which provides a tunable arm for probe development,

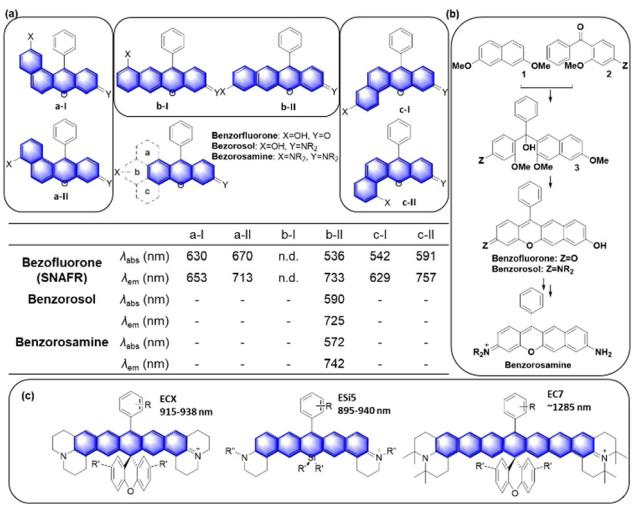

		a-I	a-II	b-I	b-II	c-I	c-II
Bezofluorone (SNAFR)	λ_{abs} (nm)	630	670	n.d.	536	542	591
	λ_{em} (nm)	653	713	n.d.	733	629	757
Benzorosol	λ_{abs} (nm)	-	-	-	590	-	-
	λ_{em} (nm)	-	-	-	725	-	-
Benzorosamine	λ_{abs} (nm)	-	-	-	572	-	-
	λ_{em} (nm)	-	-	-	742	-	-

Fig. 11 (a) Structures of the benzofluorone, benzorosol and benzorosamine dyes. (b) Synthetic scheme of the linear benzofluorone, benzorosol and benzorosamine dyes. (c) Structures of **ECX**, **ESi5** and **EC7** dyes featuring extensive ring fusion.

was also synthesized. Notably, the linear benzorosol and benzorosamine dyes have high chemo- and photo-stability and emit in the NIR region in cells. Recently, Yang and co-workers unveiled an innovative ring-fusion strategy for the construction of highly intricate fluorophores with extensive ring structures. Employing a symmetrical approach to ring-fusion, they successfully synthesized a set of exquisitely π-conjugated dyes, namely **ECX**, **ESi5** and **EC7** (Fig. 11c).[51] **ECX**, with its five fused rings, outperformed the benzorosamine that emits at ~740 nm by significantly pushing the emission maximum to ~920 nm. **ESi5** dyes, which have a modifiable arm attached to the amine sides and bear a central Si atom, display emissions across the range of 895–940.[52] Subsequently, the same group further extended the core to seven fused rings, resulting in **EC7** dyes,[53] which pushed the emission wavelength even up to 1285 nm. These dyes have immense potential for clinical applications, allowing for enhanced light penetration within biological systems.

2.2.4. CFPX-based bioimaging probes, selected examples. Developing activatable probes based on the carboxyl-free phenyl-substituted xanthene dyes, such as rosol and rosamine dyes, requires an extra group that can quench or change their fluorescence signals. A popular approach is to introduce a reactive group, which also acts as a quencher through the PeT process, at the N/O site or phenyl site. Upon interaction with a target analyte, the attached group undergoes a cleavage reaction, restoring the dye's fluorescence. Such turn-on type fluorescence probes have been developed for cuprous ions (**F8–F10**, Fig. 12a),[42] formaldehyde (**F11**, Fig. 12a),[54] azoreductase (**F12**, Fig. 12a),[55] and peroxynitrite (**F13**, Fig. 12a).[56]

Another popular approach is to introduce an activatable group into the dyes in such a way that its introduction causes a change in intramolecular charge-transfer (ICT). The detachment of the reactive group by the target analyte can cause fluorescence signal changes. When the hydroxyl group of rosol and fluorone dyes is protected by the reactive group (R_g), the resulting probes mostly become nonfluorescent (ICT-off state). The activation/cleavage of R_g upon the interaction with the target analyte leads to a turn-on fluorescence response (ICT-on), as exemplified by an esterase probe **F14** (Fig. 12b).[57] The ICT modulation approach can be also explored for the labelling of biomolecules, as exemplified by rosol **F15** (Fig. 12c), which allows lymphatic mapping.[41] The commonly observed ICT- or PeT-off state of *O*-blocked rosol dyes can be tuned into the ICT- or PeT-on state by extending the conjugation length of dyes. The benzorosol (BRosol) dye system developed by Ahn and co-workers provides emissive derivatives even when the hydroxyl group is functionalized into its *O*-acyl or *O*-ethereal derivatives[49] or connected with a typical PeT quencher (nitrophenyl or quinone groups).[49,58] The further π-conjugation keeps the localized excited states of the *O*-functionalized derivatives still emissive. Also, π-conjugation causes a lowering of the LUMO energy, effectively prohibiting the otherwise feasible occurrence of the PeT process. Notably, there is a large difference in emission wavelength between the phenolic (λ_{em} = 590 nm) and phenolate (λ_{em} = 725 nm) forms of BRosol, which

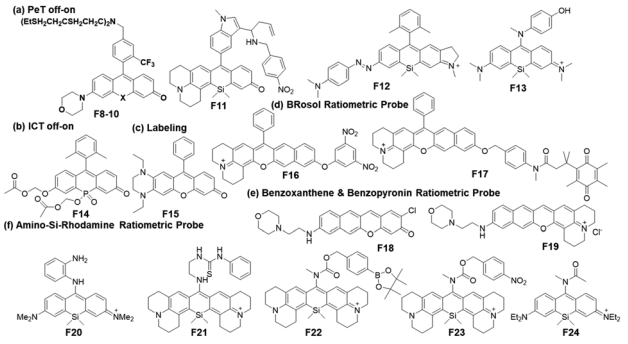

№	Abs/Em (nm)	Application
F8	$\lambda_{abs}/_{em}$: 516/608; Aqueous solution; X=CMe_2	
F9	$\lambda_{abs}/_{em}$: 568/638; Aqueous solution; X=$SiMe_2$	Cu sensing; HEK 293T, MEF cells (Turn-on)
F10	$\lambda_{abs}/_{em}$: 569/679; Aqueous solution; X=POPh	
F11	PRD: $\lambda_{abs}/_{em}$: 633/649; PBS (pH 7.4)	Formaldehyde Sensing; HEK293TN, NS1 cells; (Turn-on)
F12	PRD $\lambda_{abs}/_{em}$: 637/660; PBS (pH 7.4)	Hypoxia bioreductases; A549 cells; *in vivo* mouse Imaging; (Turn-on)
F13	PRD: $\lambda_{abs}/_{em}$: 460/610; PBS (pH 7.4)	Peroxynitrite Sensing; Two-photon; HepG2, RAW264.7, COS-7 cells; Rat tissue Imaging (Heart, kidney); *in vivo* tumor-bearing mouse xenograft; (Turn-on)
F14	PRD: $\lambda_{abs}/_{em}$: 600/619; PBS (pH 7.4)	PLE Sensing; HeLa cells; (Turn-on)
F15	PRB: $\lambda_{abs}/_{em}$: 550/710; PBS (pH 7.4)	Lymphatic mapping; GBM U87 cells; *in vivo* tumor-bearing mouse xenograft; (Labeling)
F16	PRB: $\lambda_{abs}/_{em}$: 460/590; PRD: $\lambda_{abs}/_{em}$: 615/725; PBS (pH 7.4, 30% EtOH)	GSH Sensing; HeLa cells; Mouse tissue imaging (Liver); (Ratiometric)
F17	PRB: $\lambda_{abs}/_{em}$: 520/590; PRD: $\lambda_{abs}/_{em}$: 650/725; PBS (pH 7.4, 0.1 M KCl, 0.007% BSA)	hNQO1 Sensing; A549, HT29 cells; Mouse tissue imaging (Muscle, lung, testis, Urinary bladder, colon, kidney, stomach); (Ratiometric)
F18	PRB: $\lambda_{abs}/_{em}$: 540/685; PRD: $\lambda_{abs}/_{em}$: 408/510; PBS (pH 5.0, 30% EtOH)	Lysosomal Cys Sensing; Two-photon; HeLa cells; (Ratiometric)
F19	PRB: $\lambda_{abs}/_{em}$: 613/704; PRD: $\lambda_{abs}/_{em}$: 426/512; PBS (pH 5.0, 30% EtOH)	Lysosomal Bisulfite Sensing; Two-photon; HeLa cells; (Ratiometric)
F20	PRB: $\lambda_{abs}/_{em}$: 450/610; PRD: $\lambda_{abs}/_{em}$: 515/710; HEPES (pH 7.4, 30% ACN)	Nitric oxide Sensing; HeLa cells; (Ratiometric)
F21	PRB: $\lambda_{abs}/_{em}$: 504/642; PRD: $\lambda_{abs}/_{em}$: 710/717; PBS (pH 7.4, 20% DMF)	HOCl Sensing; RAW264.7 cells; Mouse tissue imaging (Brain); (Ratiometric)
F22	PRB: $\lambda_{abs}/_{em}$: 702/712; PRD: $\lambda_{abs}/_{em}$: 481/655; PBS (pH 7.4)	H_2O_2Sensing; Two-photon; A549 cells; (Ratiometric)
F23	PRB: $\lambda_{abs}/_{em}$: 703/710; PRD: $\lambda_{abs}/_{em}$: 486/655; PBS (pH 7.4)	NTR Sensing; Two-photon; A549 cells; IVIS mouse organ images (Lungs, heart, spleen, kidney, liver); Mouse tissue imaging (kidney); (Ratiometric)
F24	HCl (1 mM): $\lambda_{abs}/_{em}$: 663/683; NaOH (1 mM): $\lambda_{abs}/_{em}$: 400/605	pH Sensing; (Labeling)

Fig. 12 Selected examples of fluorescent probes developed from the rosol, rosamine, fluorone, benzoxanthene, benzopyronin and amino-Si-rhodamine dyes: probes' basic optical properties and target analytes.

offers an excellent ratiometric sensing platform to sense GSH (**F16**, Fig. 12d)[49] and hNQO1 (**F17**, Fig. 12d).[58]

In 2019, Gryko and co-workers reviewed the synthesis, photophysical properties and applications of rhodol (and rosol) as fluorescent probes. They predicted the development of a π-extended rhodol compound (Fig. 12e, benzoxanthene), which was successfully prepared in 2020, along with its amine analogue (Fig. 12e, benzopyronin). Taking advantage of the fact that the skeleton can be readily attacked by nucleophilic analytes through 1,6-conjugate addition, they were developed into fluorescent probes for cysteine (Cys) (**F18**, Fig. 12e) and[59] bisulfite (**F19**, Fig. 13e).[60]

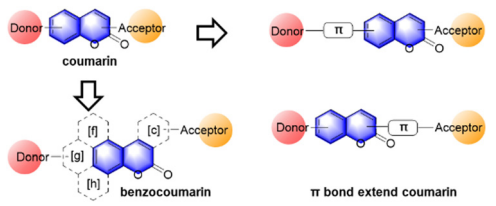

Fig. 13 Strategies to make coumarin absorption/emission wavelength bathochromic-shift.

As we have mentioned above, the probes based on the amino-Si-rhodamine system can be developed into probes that show either hypsochromic (Fig. 10b) or bathochromic (Fig. 10c) emission spectral shifts, depending on the probe design: the probes for H_2O_2 (**F20**, Fig. 12f),[46] NTR (**F21**, Fig. 12f),[61] and pH (**F22**, Fig. 12f)[62] exhibit hypsochromic signal changes, whereas those for nitric oxide (**F23**, Fig. 12f)[63] and HOCl (**F24**, Fig. 12f) exhibit bathochromic signal changes.[64]

2.3. Xanthene derivatives: summary

In the above subchapters, we have overviewed and discussed strategies toward the emission bathochromic shift applied to the xanthene fluorophores, such as rhodamine, fluorescein, and their analogues. Commonly used approaches are ring fusion, central atom replacement, and variation of the amino donor. The replacement of the primary amino group (rhodamine 123) with a tertiary amino group (rhodamine 630) results in the emission maximum shift from 532 nm to 616 nm ($\Delta\lambda$ = 84 nm; ethanol). The central O atom replacement of a rhodamine dye to Si and P results in the emission maximum shift from 571 nm to 664 nm ($\Delta\lambda$ = 93 nm) and 723 nm ($\Delta\lambda$ = 152 nm) in pH 7.3 HEPES, respectively (Fig. 5). The linear fusion of one benzene ring to rhodamine B led to a benzorhodamine (**b-II**, Fig. 6), which resulted in the emission maximum shift from 576 nm to 785 nm ($\Delta\lambda$ = 209 nm; rhodamine B in EtOH, benzorhodamine in 30% EtOH/PBS). The ring-fusion approach is highly effective for the emission bathochromic shift, as highlighted by the seven ring-fused EC7 dyes that emit at ~1285 nm.

3. Coumarin

Considering that the coumarins are typical ICT dyes, we can induce bathochromic shifts in their emission wavelength by increasing the donor/acceptor's ability, in addition to extending the π-conjugation length.

In 1984, Jones and co-workers investigated the photophysical properties of coumarin dyes with several different electron-donor and -acceptor groups.[65] However, the modification of the donor and acceptor alone is not sufficient to make the coumarin emit at more than 600 nm (λ_{em}). Therefore, π extension is required to generate coumarin derivatives emitting in the red/far-red or NIR region.

3.1. Benzocoumarins

3.1.1 Robust ring-fusion stratagem. Various benzocoumarin dyes have been reported,[66–68] which can be categorized by the ring-fusion geometry: benzo[*c*]coumarins, benzo[*f*]coumarins, benzo[*g*]coumarins and benzo[*h*]coumarins (Fig. 13a). Among them, benzo[*g*]coumarins emit in longer wavelengths than the others, and are thus promising for bioimaging applications.[68]

In 2017, Ahn and co-workers designed a novel strategy to modify a typical D–A coumarin dye to far-red emitting benzo[*g*]-coumarins.[4] The emission maximum data (Fig. 13b) indicate that the π-system extension causes a greater spectral bathochromic

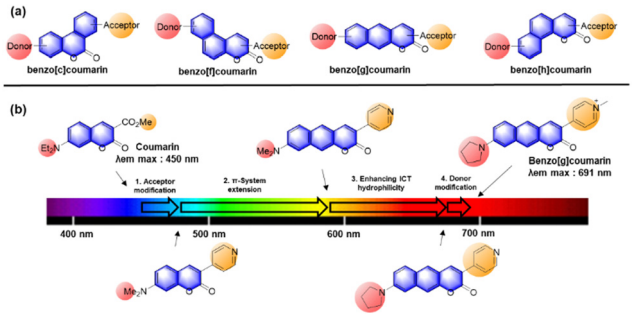

Fig. 14 (a) Different types of benzocoumarin. (b) Structural modification of a coumarin dye (data collected in EtOH).

shift compared to donor/acceptor modifications. Through a series of modifications (Fig. 14b), a bathochromic emission spectral shift of 241 nm was obtained (in EtOH) compared to that of the original coumarin.

3.1.2. Bioimaging probes based on benzocoumarins. The pyridinium-benzocoumarin dyes emit in the near-infrared (NIR) wavelength region and have good TP properties and thus have been used for deep-tissue imaging (**F25**, Fig. 15a).[4] By introducing a mitochondria-targeting moiety such as triphenylphosphonium ($-PPh_3^+$), a benzocoumarin dye has been used for monitoring mitochondrial trafficking (**F26**, Fig. 15a).[69] In 2020, a systematic study on the photophysical brightness of benzocoumarin dyes in different media revealed that benzothiazole–benzocoumarin dyes are super-bright in cells in

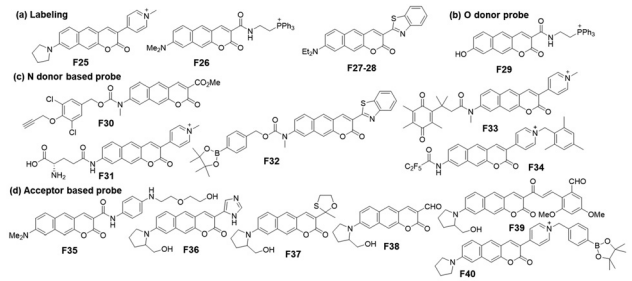

№	Abs/Em (nm)	Application
F25	PRB: $\lambda_{abs}/_{em}$: 527/691; EtOH	Deep tissue imaging; Two-photon; Mouse tissue imaging (Brain, kidney, liver, lung, spleen); (labeling)
F26	PRB: $\lambda_{abs}/_{em}$: 470/626; PBS (pH 7.4)	Mitochondria trafficking sensing; Two-photon; HeLa, T98G cells; Rat tissue imaging (Hippocampal tissue); (labeling)
F27 F28	PRB: $\lambda_{abs}/_{em}$: 492/625; MeCN	Super-bright imaging; HeLa, HEK293T, MCF-7, A549 cells Lipid droplets sensing; 3T3-L1, HeLa cells; FLIM mouse images (Livers, subcutaneous); (labeling)
F29	pH 4: $\lambda_{abs}/_{em}$: 370/540; pH 10: $\lambda_{abs}/_{em}$: 453/604	Mitochondrial pH sensing; Two-photon; HeLa cells; Rat tissue imaging (Hippocampal tissue); (labeling)
F30	PRB: $\lambda_{abs}/_{em}$: 350/530; PRD: $\lambda_{abs}/_{em}$: 450/600; MeCN:H_2O=1:9	Pd sensing; A549 cells; (Ratiometric)
F31	PRB: $\lambda_{abs}/_{em}$: 390/570; PRD: $\lambda_{abs}/_{em}$: 450/640; PBS (pH 7.4)	GGT sensing; Two-photon; HeLa cells; Mouse tissue imaging (Kidney, small intestine, brain, liver, stomach, pancreas, tumour); (Ratiometric)
F32	PRB: $\lambda_{abs}/_{em}$: 380/520; PRD: $\lambda_{abs}/_{em}$: 480/610; PBS (pH 7.4, 50% EtOH)	H_2O_2 sensing; Two-photon; HeLa cells; Mouse tissue imaging (Tumour); IVIS images (Mouse tumor colon); (Ratiometric)
F33	PRB: $\lambda_{abs}/_{em}$: 360/555; PRD: $\lambda_{abs}/_{em}$: 470/650; PBS (pH 7.4, 0.1 M KCl, 0.007% BSA)	hNQO1 sensing; Two-photon; HT29 cells; (Ratiometric)
F34	PRB: $\lambda_{abs}/_{em}$: 380/555; PBD: $\lambda_{abs}/_{em}$: 410/650; PBS (pH 7.4)	Elastase sensing; Two-photon; A549 cells; Mouse tissue imaging (IBD mouse model); (Ratiometric)
F35	PRD: $\lambda_{abs}/_{em}$: 473/613; PBS (pH 7.4, 10% MeCN)	Nitric oxide sensing; Two-photon; HepG2, RAW264.7 cells; Mouse tissue imaging (Kidney); (Turn-on)
F36	pH 4: $\lambda_{abs}/_{em}$: 450/620; pH 5: $\lambda_{abs}/_{em}$: 340/480	Extreme acidity sensing; *E. Coli* cells; (Labeling)
F37	PRB: $\lambda_{abs}/_{em}$: 424/598; PRD: $\lambda_{abs}/_{em}$: 487/633; PBS (pH 7.4)	HOCl sensing; Two-photon; HeLa cells Mouse tissue imaging (Brain); (Ratiometric)
F38	PRB: $\lambda_{abs}/_{em}$: 487/625; PBD: $\lambda_{abs}/_{em}$: 430/562; PBS (pH 7.4)	Bisulfite sensing; Two-photon; HeLa cells; (Ratiometric)
F39	PRD: $\lambda_{abs}/_{em}$: 485/628; MeCN:H_2O=1:9	H_2S sensing; HeLa cells; (Turn-on)
F40	PRB: $\lambda_{abs}/_{em}$: 520/642; PBD: $\lambda_{abs}/_{em}$: 425/593; PBS (pH 7.4)	H_2O_2 sensing; Two-photon; HeLa cells; Mouse tissue imaging (Inflammation-induced); (Ratiometric)

Fig. 15 Applications of benzo[*g*]coumarins to develop fluorescent probes and their basic optical properties and target analytes summarized.

comparison with typical conventional dyes (**F27**, Fig. 14a).[70] The work also highlights that the cellular environment offers the third space for organic fluorophores in addition to organic and aqueous media.[71] The dipolar nature of benzocoumarin dyes, specifically in the case of **F28**, makes it useful in detecting lipid droplets.[72]

Because the benzocoumarin core is rather difficult to functionalize, the probe design is mainly conducted by modification of the donor (hydroxyl or amino) or acceptor (carboxyl) groups. In 2016, a hydroxy-benzocoumarin dye was utilized for pH sensing, as its hydroxyl and alkoxy ($-OH/-O^-$) forms exhibit different photophysical properties (**F29**, Fig. 15b).[73]

In the case of benzocoumarins bearing an amino donor ($-NRR'$) at the 7-position, modification of them into amide or carbamate derivatives commonly leads to a change in their ICT properties. These properties can be used to develop reaction-based ratiometric probes: accordingly, several ratiometric probes have been developed for sensing Pd (**F30**, Fig. 15c),[74] GGT (**F31**, Fig. 15c),[75] H_2O_2 (**F32**, Fig. 15c),[76] hNQO1 (**F33**, Fig. 15c),[77] and elastase (**F34**, Fig. 15c).[78]

Similarly, ratiometric probes can be developed by modifying the acceptor site, leading to probes for sensing nitric oxide (**F35**, Fig. 15d),[79] extreme acidity (**F36**, Fig. 15d),[80] HOCl (**F37**, Fig. 15d),[81] bisulfite (**F38**, Fig. 15d),[82] H_2S (**F39**, Fig. 15d),[83] and H_2O_2 (**F40**, Fig. 15d).[84]

3.2 Vinyl-extended coumarins

3.2.1. Vinyl extension stratagem. Instead of the ring fusion to extend the electron delocalization as shown with benzocoumarins, we can also extend pi-conjugation simply by inserting vinyl groups between the C-3 substituent and the coumarin ring, although such an approach does not guarantee that the vinyl-containing acceptors have sufficient stability to certain reactive biological species (reactive oxygen and nitrogen species) and also to photochemical reactions.[85] Not only the vinyl group[86] but also other groups are possible for the pi-extension, such as alkynyl,[87] thiazole,[88] thiophene,[89] benzothiadiazole,[90] or a combination of them.[91] For example, when a coumarin was subjected to the vinyl extension strategy with a pyridinium acceptor, its emission maximum was red-shifted from 450 nm to 650 nm. An extensive vinyl extension reported by Avhad and co-workers further pushed the emission maximum up to 756 nm (Fig. 16).[89] Note that for such an extensive vinyl extension, a powerful electron-acceptor group is required to induce sufficient ICT and thus significant emission red-shift.

As noted above, the vinyl-extension strategy (Fig. 16) can make the resulting electron-acceptor moiety vulnerable to both

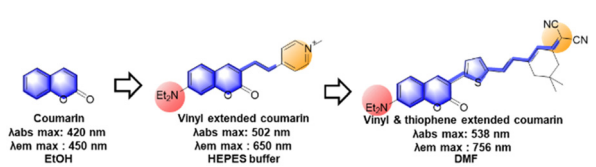

Fig. 16 Transforming coumarin into a NIR-emitting dye through an extensive vinyl extension.

nucleophilic and electrophilic species, such as bisulfite, biothiols, hypochlorous acid, peroxynitrite, *etc.* The chemical and photochemical stability of the vinyl-containing acceptors including hemicyanine moieties seems to be dependent on the whole dye system: the vinyl-extended coumarins bearing 2-indolinum or 2-benzothiazolium groups are not chemically and photochemically stable, whereas those of the 4-pyridinium group have sufficient chemo- and photo-stability.[85] Besides, the free bond rotation around the vinyl group provides the resulting dyes with viscosity- and polarity-sensitive emission behaviour, leading to fluorescent probes for these environmental parameters.[92]

3.2.2 Bioimaging probes based on vinyl-extended coumarins. The vinyl-extended coumarin fluorophores can be classified into four types based on their application modes. They can be used for labelling purposes; in this case, there are no structural changes during fluorescence monitoring (Fig. 17a). They are used for staining DNA and related biomolecules (**F41–F43**, **F48** & **F49**, Fig. 17a),[93–98] binding-induced heparin sensing (**F44**, Fig. 17a),[99] and polarity sensing (**F45** & **F46**, Fig. 17a).[100] If there is a basic nitrogen-containing heterocycle in the electron-acceptor side, such as indole or quinolone, protonation leads to a change in the fluorescence signal and thus such dyes can be used for pH sensing (**F50–F52**, Fig. 17b).[101,102] Besides, a vinyl-extended coumarin bearing a 2,3-dihydroindole, which can react with hydroxyl radicals to form a more stable 2-indolinum was used for monitoring of hydroxyl radicals (**F53** & **F54**, Fig. 17b).[103,104]

The most popular use of such vinyl-extended coumarins is found in sensing of nucleophilic species, such as bisulfite (**F55–F57**, **F59**, **F60** & **F65**, Fig. 17c),[105–110] cysteine (**F58**, Fig. 17c),[111] cyanide (**F61**, **F63**, **F64** & **F67**, Fig. 17c),[112–115] hydrogen sulfide (**F62**, Fig. 17c),[116] and hydrazine (**F66**, Fig. 17c).[117] Note that these hemicyanine moieties may also undergo electrophilic reactions with hypochlorous acid or peroxynitrite,[85] which warrant careful interference analysis against these species.

For the last type, it is also possible to cause a fluorescence signal change by further decorating the acceptor part (Fig. 17d), as shown in the detection of esterase (**F68**, Fig. 17d),[118] cysteine (**F69**, Fig. 17d)[119] and benzoyl peroxide (**F70**, Fig. 17d).[120]

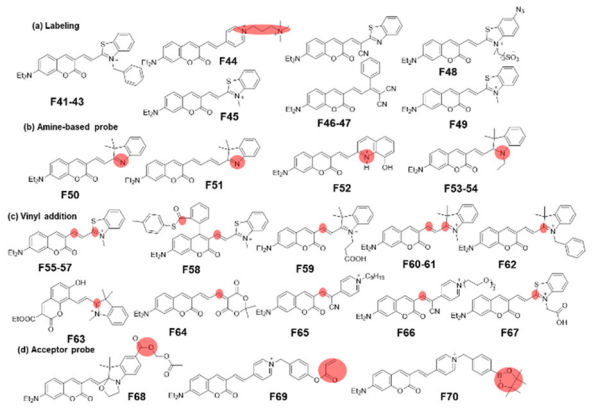

№	Abs/Em (nm)	Application
F41	PRB: $\lambda_{abs}/_{em}$: 426, 561/467, 642; MeOH	Mitochondrial Polarity sensing; MCF-7, RAW 264.7, COS-7, HeLa, HepG2 cells; (Labeling)
F42	PRD: $\lambda_{abs}/_{em}$: 553/650; Tris-acetate buffer (pH 6.7)	G-quadruplex Sensing; (Turn-on)
F43	PRD: $\lambda_{abs}/_{em}$: 561/650; MeOH	G-quadruplex Sensing; (Turn-on)
F44	PRB: $\lambda_{abs}/_{em}$: 502/650; HEPES (pH 7.4)	Heparin sensing; (Turn-off)
F45	PRD: $\lambda_{abs}/_{em}$: 521/610; Tris-HCl buffer (pH 7.4)	AT-Base Pair Detection; HEK 293T cells; (Turn-on)
F46	PRB: $\lambda_{abs}/_{em}$: 527/605; DMF	Polarity Sensing; (Labeling)
F47	PRB: $\lambda_{abs}/_{em}$: 528/634; DMF	Polarity Sensing; (Labeling)
F48	PRB: $\lambda_{abs}/_{em}$: 548/653; PRD: $\lambda_{abs}/_{em}$: 567/655; PBS	Nucleic acid labeling; HeLa cells; (Labeling)
F49	PRD: $\lambda_{abs}/_{em}$: 575/625; Tris-HCl buffer (60 mM KCl, pH 7.4)	G-quadruplex sensing; HeLa cells; (Turn-on)
F50	pH 2.0: $\lambda_{abs}/_{em}$: 559/648; pH 7.0: basic: $\lambda_{abs}/_{em}$: 469/562; Buffer (25% MeCN)	pH sensing, lysosome localization; KB cells; (Labeling)
F51	pH 1.5: $\lambda_{abs}/_{em}$: 572/722; pH 7.0: $\lambda_{abs}/_{em}$: 474/600; Buffer (30% MeCN)	
F52	pH 2.9: $\lambda_{abs}/_{em}$: 452/544; pH 7.4: $\lambda_{abs}/_{em}$: 516/644; Aqueous solution (50% MeOH)	pH probe; HeLa, Tca-8113 cells; (Labeling)
F53	PRB: $\lambda_{abs}/_{em}$: 408/495; PRD: $\lambda_{abs}/_{em}$: 575/651; H_2O (50% MeOH)	Hydroxyl radicals sensing; HeLa cells; (Ratiometric)
F54		Hydroxyl radicals sensing; *P. falciparum* red Blood cells; (Ratiometric)
F55		SO_3^{2-} sensing; HeLa cells; (Ratiometric)
F56	PRB: $\lambda_{abs}/_{em}$: 545/633; PRD: $\lambda_{abs}/_{em}$: 410/478; PBS (pH 7.4)	SO_3^{2-} sensing; Two-photon; *E. Cloacae* (MTCC 509) cells; (Ratiometric)
F57		SO_4^{2-} sensing; A549 cells; (Ratiometric)
F58	PRB: $\lambda_{abs}/_{em}$: 550/644; PRD: $\lambda_{abs}/_{em}$: 405/494; PB (pH 7.4, 10% DMF)	Cys Sensing; B16, HeLa, 786-O cells; (Ratiometric)
F59	PRB: $\lambda_{abs}/_{em}$: 577/655; PRD: $\lambda_{abs}/_{em}$: 423/481; PBS (pH 7.4)	SO_2 sensing, mitochondria targeting; HepG2 cells; (Ratiometric; Labeling)
F60	PRB: $\lambda_{abs}/_{em}$: 570/650; PRD: $\lambda_{abs}/_{em}$: 420/480; PBS (pH 7.4, 15% EtOH)	SO_3^{2-} sensing, Mitochongria-targeting; HeLa cells; (Ratiometric, Labeling)
F61	PRB: $\lambda_{abs}/_{em}$: 570/630; PRD: $\lambda_{abs}/_{em}$: 415/514; Tris–HCl buffer (pH 9.3, 10% MeOH)	CN^- sensing; (Ratiometric)
F62	PRB: $\lambda_{abs}/_{em}$: 588/652; PRD: $\lambda_{ex}/_{em}$: 475/510; PBS (pH 7.4, 2% DMSO)	HS^- sensing; MCF-7 cells; (Ratiometric)
F63	PRB: $\lambda_{ex}/_{em}$: 405/450; PRD: $\lambda_{ex}/_{em}$: 405/620; Na_2CO_3–$NaHCO_3$ buffer (pH 9.4, 50% MeOH)	CN^- sensing; (Ratiometric)
F64	PRB: $\lambda_{abs}/_{em}$: 551/641; PRD: $\lambda_{abs}/_{em}$: 415/491; Tris-HCl buffer (pH 7.4, 10% DMSO)	CN^- sensing; (Ratiometric)
F65	PRB: $\lambda_{abs}/_{em}$: 560/645; PRD: $\lambda_{abs}/_{em}$: 410/485; PBS (pH 7.4, 10% MeCN)	SO_2 sensing; HeLa cells; IVIS mouse imaging; (Ratiometric)
F66	PRB: $\lambda_{abs}/_{em}$: 560/640; PRD: $\lambda_{abs}/_{em}$: 450/510; PBS (pH 7.4)	N_2H_4 sensing; A549 cells; Zebrafish; (Ratiometric)
F67	PRB: $\lambda_{abs}/_{em}$: 543/624; PRD: $\lambda_{abs}/_{em}$: 455/488; H_2O (90% MeCN)	CN^- sensing; (Ratiometric)
F68	PRD: $\lambda_{abs}/_{em}$: 600/666; Sodium phosphate buffer (pH 7.4)	Esterase sensing; A549, H226 cells; (Turn-on)
F69	PRB: $\lambda_{abs}/_{em}$: 508/644; PRD: $\lambda_{abs}/_{em}$: 452/539; PBS (pH 7.4, 50% DMSO)	Cys sensing; HeLa cells; (Ratiometric)
F70	PRB: $\lambda_{abs}/_{em}$: 505/620; PRD: $\lambda_{abs}/_{em}$: 443/525; EtOH	Benzoyl peroxide sensing; L929, HeLa cells; (Ratiometric)

Fig. 17 Vinyl-extended coumarins as fluorescent probes for bioanalytes: basic optical properties and target analytes.

4. Naphthalene

4.1. Extended naphthalene

In previous work, we have disclosed how the donor group affects the emission properties of donor–acceptor type naphthalene compounds including **ACEDAN**: an amino donor that exerts little allylic 1,3-strain to the naphthalene ring and has high electron-donating capability. This endows the resulting dipolar dye with higher fluorescence in water as well as in cells.[121] By fixing the amino donor with pyrrolidine, we have changed the acceptor part into a different heterocycle. Considering the chemo- and photo-stability of the resulting hemicyanine dyes, the dye with 4-pyridinium is the dye of choice for biological applications. With such modifications, the resulting napthylvinylpridinium (**NVP**) derivative emits at

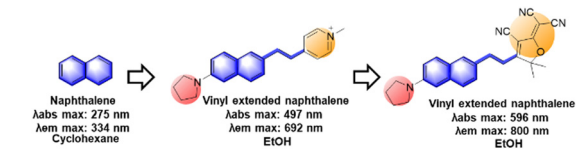

Fig. 18 Transformation of naphthalene to an NIR-emitting dye through an extensive vinyl extension.

692 nm (in ethanol), dramatically displaying a red-shift compared to naphthalene's emission at 334 nm in cyclohexane (Fig. 18). Later, Song replaced the pyridinium moiety of NVP with a tricyanofuranyl ring to form **TCFAN** (**F75** in Fig. 19). This conversion even pushes the emission maximum up to 800 nm.[92]

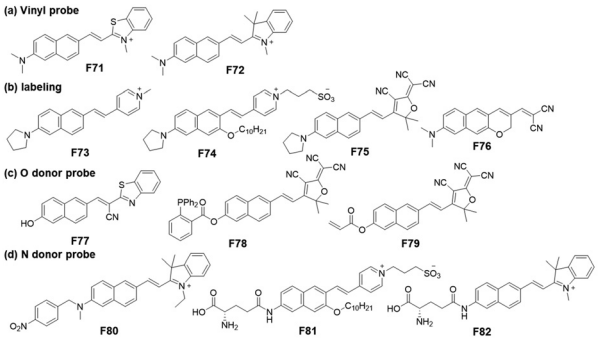

№	Abs/Em (nm)	Application
F71	PRB: $\lambda_{abs}/_{em}$: 488/690; PRD: $\lambda_{abs}/_{em}$: 360/430; PBS (pH 7.4, 5% DMSO)	SO_2 sensing; HeLa, HepG2 cells; (Ratiometric)
F72	PRB: $\lambda_{abs}/_{em}$: 525/718; PRD: $\lambda_{abs}/_{em}$: 375/535; PBS (pH 7.4)	Peroxynitrite sensing; Two-photon; A549, RAW246.7 cells; Mouse tissue imaging (Lung); (Ratiometric)
F73	PRB: $\lambda_{abs}/_{em}$: 497/692; EtOH	Biostable NIR emitting dye; Two-photon; HeLa cell; (Labeling)
F74	PRB: $\lambda_{abs}/_{em}$: 469/676; DMSO	Cell membrane sensing; Two-photon; A549 cells; Mouse tissue imaging (Spleen); (Labeling)
F75	PRB: $\lambda_{abs}/_{em}$: 596/800; EtOH	Lipid droplet sensing; HeLa, 3T3-L1 cells; (Labeling)
F76	PRD: $\lambda_{abs}/_{em}$:512/679; PBS (pH 7.4)	Amyloid-β Plaques sensing; Two-photon; HeLa cells; Mouse tissue imaging (Brain, liver, kidney, spleen, lung, cortex); (Turn-on)
F77	PRD: $\lambda_{abs}/_{em}$: 480/637; MeCN:H_2O=9:1	Hypochlorite sensing; (Turn-on)
F78	PRD: $\lambda_{abs}/_{em}$: 450/610; PBS (pH 7.4)	HNO, GSH/GSSG sensing; HepG2 cells; (Turn-on)
F79	PRD: $\lambda_{abs}/_{em}$: 480/650; PBS (pH 7.4,10% DMSO)	Cys sensing; HepG2 cells; (Turn-on)
F80	PRD: $\lambda_{abs}/_{em}$: 515/675; HEPES (pH 7.4)	NTR sensing; Two-photon; A549, SH-SY5Y cells; Zebrafish; Mouse tissue imaging (Brain); IVIS mouse imaging; (Turn-on)
F81	PRB: $\lambda_{abs}/_{em}$: 397/544; PRD: $\lambda_{abs}/_{em}$: 451/610; PBS (pH 7.4)	Membrane GGT sensing; Two-photon; HeLa, A549, HCT116, FHC, HUVEC, HEK-293T cells; Mouse tissue imaging (Thigh, colon, lung, liver, spleen, stomach, pancreas, kidney); (Ratiometric)
F82	PRB: $\lambda_{abs}/_{em}$: 426/584; PRD: $\lambda_{abs}/_{em}$: 476/654; PBS (pH 7.4)	GGT sensing; Two-photon; HCT116, HT29 cells; Human tissue imaging (Colon); (Ratiometric)

Fig. 19 Vinylnaphthalene-based fluorescent probes for bioanalytes: basic optical properties and target analytes.

4.2. Bioimaging probes based on vinylnaphthalene dyes

As mentioned above, the vinylnaphthalene-based hemicyanine dyes bearing an electron acceptor such as 2-indolinum or 2-benzothiazolium moieties have been widely used in monitoring nucleophilic analytes like bisulfite (an aqueous equilibrium species of SO_2; **F71**, Fig. 19a),[122] peroxynitrite (**F72**, Fig. 19a), *etc.*,[123] which suggest that they are susceptible to these species. Also, such hemicyanine dyes are not photochemically stable. In contrast, their 4-pyridinium analogues (NVP dyes) have good stability against many bio-analytes, including Cys, GSH, H_2O_2, HSO_3^-, HOCl, and H_2S (**F73**, Fig. 19b) as well as good photostability.[85] The NVP system was used to develop a membrane-localizing fluorophore (**F74**, Fig. 19b) and other probes.[124,125] Instead of the charged heterocycles, a charge-neutral but strong electron-withdrawing group, such as 2-(3-cyano-4,5,5-trimethyl-2(5*H*)-furanylidene)malononitrile (TCF), can be introduced to develop a NIR-emitting probe for lipid droplets, which provide a nonpolar and viscous environment to the dipolar dye (**F75**, Fig. 19b).[92] Essentially, any dipolar dyes, which show polarity (and also viscosity) sensitive emission behaviour, can be used to sense lipid droplets. Also, environment-sensitive π-extended dipolar dyes can be used to detect amyloid-β (Aβ) plaques, which provide a much less polar and congested environment to the dipolar dye compared to the case where the dye resides outside the plaques. This effect is evidenced by a robust deep red-emitting Aβ probe (**F76**, Fig. 19b).[3]

Instead of the amino donor, the hydroxyl group can act as an electron donor. Additionally, the dyes bearing such a hydroxyl donor show emission changes depending on the medium pH that governs their equilibrium between the hydroxyl and alkoxy forms. Accordingly, such 6-hydroxy-naphthalene dyes have been used to develop fluorescent probes for hypochlorite (**F77**, Fig. 19c),[126] HNO + GSH/GSSG (**F78**, Fig. 19c),[127] and Cys (**F79**, Fig. 19c).[128] On the other hand, as the fluorescent probes based on aryl alcohol (ArOH) or phenolic dyes generally show pH-dependent emission behaviour, their use in the quantitative analysis should be conducted carefully by measuring the pH-dependent emission signal change.

In the case of dipolar dyes bearing an amino donor, we can develop activatable probes by introducing an analyte-reactive moiety onto the amino group. Such functionalization of the amino donor causes a significant change in the ICT of the dyes; this property allows us to develop activatable probes, as demonstrated for NTR (**F80**, Fig. 19d)[129] and GGT (**F81** & **F82**, Fig. 19d).[130,131] When the reactive group is a fluorescence quencher, such as nitroaryl, we may observe a turn-on type fluorescence signal change. However, we may generate a ratiometric probe even in such a case wherein it could modulate the PeT energy levels by choosing an appropriate fluorophore.[77]

In the above three sections, we have described known strategies to have bathochromic emission shifts of the common fluorophores (benzene-substituted xanthene, coumarin, and naphthalene). Note that other hybrid dye systems are developed as well. Two important hemicyanine types are the **CS** dye[132] and **HD** dye[133] developed by Lin's group, which have been widely used in probe development as well as other bio-applications.[134–136] Such a hybridization approach is also a useful method to obtain deep-red/NIR-emitting fluorophores; however, none of the original fluorophore's structure has been conserved in those dye systems and thus they are excluded in this review.

5. Molecular probe design

If we set aside the probes used to detect environmental parameters such as pH, polarity, viscosity, *etc.* (for example, **F26**, **F48**, **F75**), we can classify the molecular probes into two types based on the target detection mode: (1) binding-induced and (2) reaction/activity-induced. The latter detection mode has been widely explored recently, leading to a vast number of reaction-based/activatable probes.[137–139] Note that such activatable probes provide time-lapsed accumulated concentration/activity levels, whereas the binding-based probes allow us to monitor the dynamic concentration/activity information on the target analyte. To develop the binding-based probes, we explore fluorescence signal changes (wavelength or intensity) upon binding with the target analyte. Accordingly, for developing such probes, fluorophores whose photophysical properties are sensitive to environmental changes, such as the electron push–pull type, dipolar dyes, are generally utilized. However, the rationale design of binding-based probes, in particular for enzymes, is challenging because we should consider a substrate that binds specifically to the target enzyme and the binding process should cause a fluorescence signal change. On the other hand, reaction-based probes have flourished recently,

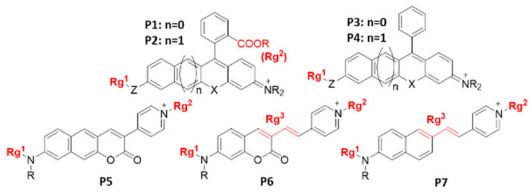

Fig. 20 Potential sites for a reactive group (R_g) in several activatable probes selected.

as benefited from a variety of chemical conversions that can be selectively executed by target analytes. We have provided selected examples of such activatable probes, which sense a variety of biologically important analytes. To develop activatable probes, we introduce a reactive group (R_g) typically at the donor or acceptor site (Fig. 20). The reactive group can be introduced to interrupt the spirolactone ring-opening process in the case of the **CPX** families (**P1**, **P2** in Fig. 20). A part of a fluorophore, such as a vinyl unit, can also be the reactive site for certain analytes (**P6**, **P7** in Fig. 20).

When the reactive group undergoes an analyte-specific chemical conversion (cleavage or conversion into another structure), it involves an ICT change, thus resulting in fluorescence signal changes. The fluorescence change can be turn-off, turn-on, or ratiometric modes depending on the reactive group and fluorophore. Even if the reactive group acts as a quencher, we can realize turn-on or ratiometric signalling by choosing an appropriate fluorophore (for example, **F4** *vs.* **F17**, **F32** *vs.* **F33**).

Another general issue to be mentioned is that as the π-conjugation length increases (for example, **P2** and **P4**), the probe may show aggregation-caused quenching (ACQ) behaviour even at the micromolar concentrations. Thus, it is always required to check the cellular aggregation behaviour of a probe for biological applications.

Also, it is necessary to secure the chemical stability of an activatable probe toward various biological analytes, particularly those containing ''reactive'' functional groups. For example, probes bearing a Michael acceptor are known to undergo conjugation addition reactions with nucleophilic biothiols (**F62**: hydrogen sulfide, **F69**: cysteine, **F78**: glutathione, *etc.*) and bisulfite anions (**F55–F57**, **F59**, F60, and **F65**). Also, probes containing an electron-rich vinyl unit are known to undergo oxidation reactions with reactive oxygen species, such as peroxynitrite (**F72**), hypochlorous acid (**F77**), *etc.*

6. Conclusion

We have analyzed the conversion strategies employed to achieve emission bathochromic shifts into the red/NIR region, starting from typical organic fluorophores based on three core structures—xanthene, coumarin, and naphthalene. Also, we have listed selected examples of how to apply these fluorophores to molecular probes for biological analytes. We believe that the strategies and their effectiveness compared here will motivate scientists to develop organic fluorophores even emitting in farther wavelengths, such as in the NIR-II region, and also serve as a valuable guide for designing red- and NIR-emitting fluorophores in the future, in addition to choosing a fluorophore in demand.

7. Perspective

(1) The red/NIR emitting fluorophores shown here have the potential for imaging biological analytes at deeper depths with less autofluorescence interference as well as reduced photodamage.

(2) We have analyzed the strategies to make three typical types of fluorophores emit in longer wavelengths, which involve electron-donor/-acceptor modifications, central atom replacement (for xanthene dyes), and conjugation length extension. A proper combination of these strategies to realize further emission wavelength shifts of known dyes and the design of new fluorophore skeletons will pave the way for the translation of fluorescent materials into medical practices in the future.

(3) Some of the known fluorophores emitting in the NIR-I or further in the NIR-II region have conformationally flexible vinyl units in their structures, which make them vulnerable to degradation by photons and chemicals. Also, the conformationally flexible nature makes them poorly emissive in aqueous media, as known with cyanine dyes. These issues should be carefully evaluated in developing fluorophores using the vinyl extension approach. In the pursuit of aromatic ring fusion, a key consideration lies in ensuring adequate solubility in biological media while mitigating the aggregation-caused quenching phenomenon. Furthermore, we must also explore cost-effective synthetic routes to complement these endeavours.

(4) A fluorophore's brightness is influenced by environmental factors, such as viscosity, polarity, pH, and hydrophobicity/hydrophilicity. As a result, it is inadequate to judge a fluorophore's potential for bioimaging application solely based on its quantum yield measured in solution. Indeed, it is not uncommon to see fluorophores with low quantum yields offering bright cellular images.

(5) In designing fluorescent probes, it is highly recommended to predict their optical behaviour (turn-on, turn-off or ratiometric response) through molecular orbital calculations before synthetic efforts. Even with a reactive group that can act as a PeT quencher, we can alleviate the quenching possibility by properly choosing a fluorophore with ''mismatched'' orbital energies for the PeT process.

(6) The selection of a fluorophore must consider compatibility with currently available optical devices. For instance, in the clinical instrument for fluorescence-guided surgery, lasers operating at 780–800 nm are extensively utilized (based on the FDA-approved ICG dye). Thus, fluorophores that can be excited within this spectral range and emit strong fluorescence have the potential for clinical experiments.

(7) Furthermore, our optimistic outlook for the future of this field encompasses advancements in multiplex imaging and sensing multiple analytes. Currently, multiplex imaging heavily relies on commonly-used emission channels, notably including

wavelengths such as 488, 555, 647, and 750 nm. To enhance convenience and efficiency in this area, we envision the incorporation of one or two additional NIR-emitting fluorophores, alongside the utilization of compatible optical instruments. This progressive approach will significantly improve the efficiency of cyclic immunofluorescence imaging, while also enabling the simultaneous staining of a greater number of biomarkers for flow cytometry. As a result, the entire process will be streamlined. Another future direction will be the development of probes for sensing multiple analytes. The current probes mostly target single analytes. Looking ahead, our focus will be on designing probes capable of detecting multiple analytes in a sense of the AND logic gate, with which we could mitigate the false-positive or -negative errors in disease diagnosis. These advancements in probe technology hold immense potential for precise disease diagnosis and detection, facilitating more accurate and comprehensive assessments in clinical settings.

Author contributions

M. D.: writing original draft; writing review & editing; investigation. Y. J. Y.: investigation. S. S.: investigation. K. H. A.: supervision, writing review & editing.

Conflicts of interest

There are no conflicts to declare.

Acknowledgements

This research was supported by the Basic Science Research Program through the National Research Foundation of Korea (NRF) funded by the Ministry of Education (NRF2019R1A2C2085438); this research was also supported by funding from the Cancer Early Detection Advanced Research (CEDAR) centre at the Oregon Health & Science University's Knight Cancer Institute. M. D. gratefully acknowledges Professor Lei G. Wang (BME department, OHSU) for the helpful discussions.

References

1 R. Liu, Y. Xu, K. Xu and Z. Dai, *Aggregate*, 2021, **2**, e23.
2 M. Monici, *Biotechnol. Annu. Rev.*, 2005, **11**, 227–256.
3 D. Kim, H. Moon, S. H. Baik, S. Singha, Y. W. Jun, T. Wang, K. H. Kim, B. S. Park, J. Jung, I. Mook-Jung and K. H. Ahn, *J. Am. Chem. Soc.*, 2015, **137**, 6781–6789.
4 Y. W. Jun, H. R. Kim, Y. J. Reo, M. Dai and K. H. Ahn, *Chem. Sci.*, 2017, **8**, 7696–7704.
5 X. Zhang, S. Bloch, W. Akers and S. Achilefu, *Curr. Protocol. Cytom.*, 2012, **Chapter 12**, 1–12.
6 M. Beija, C. A. Afonso and J. M. Martinho, *Chem. Soc. Rev.*, 2009, **38**, 2410–2433.
7 J. Arden, G. Deltau, V. Huth, U. Kringel, D. Peros and K. H. Drexhage, *J. Lumin.*, 1991, **48–49**, 352–358.
8 G. Jiang, T. B. Ren, E. D'Este, M. Xiong, B. Xiong, K. Johnsson, X. B. Zhang, L. Wang and L. Yuan, *Nat. Commun.*, 2022, **13**, 2264.
9 T. B. Ren, W. Xu, W. Zhang, X. X. Zhang, Z. Y. Wang, Z. Xiang, L. Yuan and X. B. Zhang, *J. Am. Chem. Soc.*, 2018, **140**, 7716–7722.
10 G. Jiang, X. F. Lou, S. Zuo, X. Liu, T. B. Ren, L. Wang, X. B. Zhang and L. Yuan, *Angew. Chem., Int. Ed. Engl.*, 2023, **62**, e202218613.
11 J. B. Grimm, A. J. Sung, W. R. Legant, P. Hulamm, S. M. Matlosz, E. Betzig and L. D. Lavis, *ACS Chem. Biol.*, 2013, **8**, 1303–1310.
12 K. Kolmakov, V. N. Belov, C. A. Wurm, B. Harke, M. Leutenegger, C. Eggeling and S. W. Hell, *Eur. J. Org. Chem.*, 2010, 3593–3610, DOI: **10.1002/ejoc.201000343**.
13 Q. Zheng, A. X. Ayala, I. Chung, A. V. Weigel, A. Ranjan, N. Falco, J. B. Grimm, A. N. Tkachuk, C. Wu, J. Lippincott-Schwartz, R. H. Singer and L. D. Lavis, *ACS Cent. Sci.*, 2019, **5**, 1602–1613.
14 L. Wang, M. Tran, E. D'Este, J. Roberti, B. Koch, L. Xue and K. Johnsson, *Nat. Chem.*, 2020, **12**, 165–172.
15 J. B. Grimm, A. K. Muthusamy, Y. Liang, T. A. Brown, W. C. Lemon, R. Patel, R. Lu, J. J. Macklin, P. J. Keller, N. Ji and L. D. Lavis, *Nat. Methods*, 2017, **14**, 987–994.
16 J. B. Grimm, A. N. Tkachuk, L. Xie, H. Choi, B. Mohar, N. Falco, K. Schaefer, R. Patel, Q. Zheng, Z. Liu, J. Lippincott-Schwartz, T. A. Brown and L. D. Lavis, *Nat. Methods*, 2020, **17**, 815–821.
17 J. L. Bachman, C. I. Pavlich, A. J. Boley, E. M. Marcotte and E. V. Anslyn, *Org. Lett.*, 2020, **22**, 381–385.
18 J. Arden-Jacob, J. Frantzeskos, N. U. Kemnitzer, A. Zilles and K. H. Drexhage, *Spectrochim. Acta, Part A*, 2001, **57**, 2271–2283.
19 J. B. Grimm, T. A. Brown, A. N. Tkachuk and L. D. Lavis, *ACS Cent. Sci.*, 2017, **3**, 975–985.
20 H. Ito, Y. Kawamata, M. Kamiya, K. Tsuda-Sakurai, S. Tanaka, T. Ueno, T. Komatsu, K. Hanaoka, S. Okabe, M. Miura and Y. Urano, *Angew. Chem., Int. Ed. Engl.*, 2018, **57**, 15702–15706.
21 R. Wirth, P. Gao, G. U. Nienhaus, M. Sunbul and A. Jaschke, *J. Am. Chem. Soc.*, 2019, **141**, 7562–7571.
22 G. Lukinavicius, K. Umezawa, N. Olivier, A. Honigmann, G. Yang, T. Plass, V. Mueller, L. Reymond, I. R. Correa, Jr., Z. G. Luo, C. Schultz, E. A. Lemke, P. Heppenstall, C. Eggeling, S. Manley and K. Johnsson, *Nat. Chem.*, 2013, **5**, 132–139.
23 L. G. Wang, A. R. Montano, J. R. Combs, N. P. McMahon, A. Solanki, M. M. Gomes, K. Tao, W. H. Bisson, D. A. Szafran, K. S. Samkoe, K. M. Tichauer and S. L. Gibbs, *Nat. Chem.*, 2023, **15**, 729–739.
24 X. Zhou, R. Lai, J. R. Beck, H. Li and C. I. Stains, *Chem. Commun.*, 2016, **52**, 12290–12293.
25 T. C. Binns, A. X. Ayala, J. B. Grimm, A. N. Tkachuk, G. A. Castillon, S. Phan, L. Zhang, T. A. Brown, Z. Liu, S. R. Adams, M. H. Ellisman, M. Koyama and L. D. Lavis, *Cell Chem. Biol.*, 2020, **27**, 1063–1072.
26 T. M. McCormick, B. D. Calitree, A. Orchard, N. D. Kraut, F. V. Bright, M. R. Detty and R. Eisenberg, *J. Am. Chem. Soc.*, 2010, **132**, 15480–154803.

27 B. Calitree, D. J. Donnelly, J. J. Holt, M. K. Gannon, C. L. Nygren, D. K. Sukumaran, J. Autschbach and M. R. Detty, *Organometallics*, 2007, **26**, 6248–6257.
28 A. Chmyrov, J. Arden-Jacob, A. Zilles, K. H. Drexhage and J. Widengren, *Photochem. Photobiol. Sci.*, 2008, **7**, 1378–1385.
29 Y. Koide, Y. Urano, K. Hanaoka, T. Terai and T. Nagano, *ACS Chem. Biol.*, 2011, **6**, 600–608.
30 X. Chai, X. Cui, B. Wang, F. Yang, Y. Cai, Q. Wu and T. Wang, *Chemistry*, 2015, **21**, 16754–16758.
31 Y. Komori, S. Sugimoto, T. Sato, H. Okawara, R. Watanabe, Y. Takano, S. Kitaoka and Y. Egawa, *Sensors*, 2023, **23**, 1528.
32 M. Sibrian-Vazquez, J. O. Escobedo, M. Lowry and R. M. Strongin, *Pure Appl. Chem.*, 2012, **84**, 2443–2456.
33 M. Dai, H. Lee, Y. J. Yang, M. Santra, C. W. Song, Y. W. Jun, Y. J. Reo, W. J. Kim and K. H. Ahn, *Chemistry*, 2020, **26**, 11549–11557.
34 L. G. Wang, I. Munhenzva, M. Sibrian-Vazquez, J. O. Escobedo, C. H. Kitts, F. R. Fronczek and R. M. Strongin, *J. Org. Chem.*, 2019, **84**, 2585–2595.
35 L. Wang, C. W. Barth, M. Sibrian-Vazquez, J. O. Escobedo, M. Lowry, J. Muschler, H. Li, S. L. Gibbs and R. M. Strongin, *ACS Omega*, 2017, **2**, 154–163.
36 X. Wu, Y. Gao, W. Chi, C. Wang, Z. Xu and X. Liu, *Mater. Chem. Front.*, 2023, **7**, 1137–1145.
37 D. Kim, Q. P. Xuan, H. Moon, Y. W. Jun and K. H. Ahn, *Asian J. Org. Chem.*, 2014, **3**, 1089–1096.
38 G. J. Mao, Z. Z. Liang, J. Bi, H. Zhang, H. M. Meng, L. Su, Y. J. Gong, S. Feng and G. Zhang, *Anal. Chim. Acta*, 2019, **1048**, 143–153.
39 C. Liu, X. Jiao, Q. Wang, K. Huang, S. He, L. Zhao and X. Zeng, *Chem. Commun.*, 2017, **53**, 10727–10730.
40 Q. A. Best, A. E. Johnson, B. Prasai, A. Rouillere and R. L. McCarley, *ACS Chem. Biol.*, 2016, **11**, 231–240.
41 K. S. Hettie, J. L. Klockow, T. E. Glass and F. T. Chin, *Anal. Chem.*, 2019, **91**, 3110–3117.
42 S. Jia, K. M. Ramos-Torres, S. Kolemen, C. M. Ackerman and C. J. Chang, *ACS Chem. Biol.*, 2018, **13**, 1844–1852.
43 F. Deng, L. Liu, W. Huang, C. Huang, Q. Qiao and Z. Xu, *Spectrochim. Acta, Part A*, 2020, **240**, 118466.
44 Y. Koide, Y. Urano, K. Hanaoka, T. Terai and T. Nagano, *J. Am. Chem. Soc.*, 2011, **133**, 5680–5682.
45 Z. Mao, H. Jiang, X. Song, W. Hu and Z. Liu, *Anal. Chem.*, 2017, **89**, 9620–9624.
46 K. H. Kim, S. Singha, Y. W. Jun, Y. J. Reo, H. R. Kim, H. G. Ryu, S. Bhunia and K. H. Ahn, *Chem. Sci.*, 2019, **10**, 9028–9037.
47 Y. Kushida, T. Nagano and K. Hanaoka, *Analyst*, 2015, **140**, 685–695.
48 Y. Yang, M. Lowry, X. Xu, J. O. Escobedo, M. Sibrian-Vazquez, L. Wong, C. M. Schowalter, T. J. Jensen, F. R. Fronczek, I. M. Warner and R. M. Strongin, *Proc. Natl. Acad. Sci. U. S. A.*, 2008, **105**, 8829–8834.
49 M. Dai, Y. J. Reo, C. W. Song, Y. J. Yang and K. H. Ahn, *Chem. Sci.*, 2020, **11**, 8901–8911.
50 Y. M. Poronik, K. V. Vygranenko, D. Gryko and D. T. Gryko, *Chem. Soc. Rev.*, 2019, **48**, 5242–5265.
51 Z. Lei, X. Li, X. Luo, H. He, J. Zheng, X. Qian and Y. Yang, *Angew. Chem., Int. Ed. Engl.*, 2017, **56**, 2979–2983.
52 J. Li, Y. Dong, R. Wei, G. Jiang, C. Yao, M. Lv, Y. Wu, S. H. Gardner, F. Zhang, M. Y. Lucero, J. Huang, H. Chen, G. Ge, J. Chan, J. Chen, H. Sun, X. Luo, X. Qian and Y. Yang, *J. Am. Chem. Soc.*, 2022, **144**, 14351–14362.
53 R. Wei, Y. Dong, X. Wang, J. Li, Z. Lei, Z. Hu, J. Chen, H. Sun, H. Chen, X. Luo, X. Qian and Y. Yang, *J. Am. Chem. Soc.*, 2023, **145**, 12013–12022.
54 A. Roth, H. Li, C. Anorma and J. Chan, *J. Am. Chem. Soc.*, 2015, **137**, 10890–10893.
55 K. Hanaoka, Y. Kagami, W. Piao, T. Myochin, K. Numasawa, Y. Kuriki, T. Ikeno, T. Ueno, T. Komatsu, T. Terai, T. Nagano and Y. Urano, *Chem. Commun.*, 2018, **54**, 6939–6942.
56 H. Zhang, J. Liu, L. Wang, M. Sun, X. Yan, J. Wang, J. P. Guo and W. Guo, *Biomaterials*, 2018, **158**, 10–22.
57 Y. Fang, G. N. Good, X. Zhou and C. I. Stains, *Chem. Commun.*, 2019, **55**, 5962–5965.
58 Y. J. Yang, M. Dai, Y. J. Reo, C. W. Song, S. Sarkar and K. H. Ahn, *Anal. Chem.*, 2021, **93**, 7523–7531.
59 U. Tamima, C. W. Song, M. Santra, Y. J. Reo, H. Banna, M. R. Islam and K. H. Ahn, *Sens. Actuators, B*, 2020, **322**, 128588.
60 U. Tamima, M. Santra, C. W. Song, Y. J. Reo and K. H. Ahn, *Anal. Chem.*, 2019, **91**, 10779–10785.
61 S. Sarkar, H. Lee, H. G. Ryu, S. Singha, Y. M. Lee, Y. J. Reo, Y. W. Jun, K. H. Kim, W. J. Kim and K. H. Ahn, *ACS Sens.*, 2021, **6**, 148–155.
62 P. Horváth, P. Šebej, D. Kovář, J. Damborský, Z. Prokop and P. Klán, *ACS Omega*, 2019, **4**, 5479–5485.
63 J. Tang, Z. Guo, Y. Zhang, B. Bai and W. H. Zhu, *Chem. Commun.*, 2017, **53**, 10520–10523.
64 K. H. Kim, S. J. Kim, S. Singha, Y. J. Yang, S. K. Park and K. H. Ahn, *ACS Sens.*, 2021, **6**, 3253–3261.
65 B. P. Czech and R. A. Bartsch, *J. Org. Chem.*, 1984, **49**, 4076–4078.
66 H. N. Lv, P. F. Tu and Y. Jiang, *Mini. Rev. Med. Chem.*, 2014, **14**, 603–622.
67 M. Tasior, D. Kim, S. Singha, M. Krzeszewski, K. H. Ahn and D. T. Gryko, *J. Mater. Chem. C*, 2015, **3**, 1421–1446.
68 Y. Jung, J. Jung, Y. Huh and D. Kim, *J. Anal. Methods Chem.*, 2018, **2018**, 5249765.
69 A. R. Sarkar, C. H. Heo, H. W. Lee, K. H. Park, Y. H. Suh and H. M. Kim, *Anal. Chem.*, 2014, **86**, 5638–5641.
70 Y. J. Reo, Y. W. Jun, S. W. Cho, J. Jeon, H. Roh, S. Singha, M. Dai, S. Sarkar, H. R. Kim, S. Kim, Y. Jin, Y. L. Jung, Y. J. Yang, C. Ban, J. Joo and K. H. Ahn, *Chem. Commun.*, 2020, **56**, 10556–10559.
71 K. H. Ahn and Y. W. Jun, *Phys. Sci.*, 2022, 126–129, DOI: **10.26904/RF-141-2648143398**.
72 T. Yoshihara, R. Maruyama, S. Shiozaki, K. Yamamoto, S. I. Kato, Y. Nakamura and S. Tobita, *Anal. Chem.*, 2020, **92**, 4996–5003.
73 A. R. Sarkar, C. H. Heo, L. Xu, H. W. Lee, H. Y. Si, J. W. Byun and H. M. Kim, *Chem. Sci.*, 2016, **7**, 766–773.
74 S. W. Cho, Y. J. Reo, S. Sarkar and K. H. Ahn, *Bull. Korean Chem. Soc.*, 2020, **42**, 135–139.

75 Y. J. Reo, Y. W. Jun, S. Sarkar, M. Dai and K. H. Ahn, *Anal. Chem.*, 2019, **91**, 14101–14108.
76 S. W. Cho, Y. W. Jun, Y. J. Reo, S. Sarkar and K. H. Ahn, *Results Chem.*, 2021, **3**, 100117.
77 M. Dai, C. W. Song, Y. J. Yang, H. R. Kim, Y. J. Reo and K. H. Ahn, *Sens. Actuators, B*, 2021, **330**, 129277.
78 S. Sarkar, A. Shil, M. Nandy, S. Singha, Y. J. Reo, Y. J. Yang and K. H. Ahn, *Anal. Chem.*, 2022, **94**, 1373–1381.
79 Z. Mao, H. Jiang, Z. Li, C. Zhong, W. Zhang and Z. Liu, *Chem. Sci.*, 2017, **8**, 4533–4538.
80 H. Kim, S. Sarkar, M. Nandy and K. H. Ahn, *Spectrochim. Acta, Part A*, 2021, **248**, 119088.
81 Y. W. Jun, S. Sarkar, S. Singha, Y. J. Reo, H. R. Kim, J. J. Kim, Y. T. Chang and K. H. Ahn, *Chem. Commun.*, 2017, **53**, 10800–10803.
82 U. Tamima, S. Singha, H. R. Kim, Y. J. Reo, Y. W. Jun, A. Das and K. H. Ahn, *Sens. Actuators, B*, 2018, **277**, 576–583.
83 M. Santra, S. Sarkar, Y. W. Jun, Y. J. Reo and K. H. Ahn, *Tetrahedron Lett.*, 2018, **59**, 3210–3213.
84 H. R. Kim, S. Sarkar and K. H. Ahn, *Chem. – Asian J.*, 2022, **17**, e202101317.
85 H. J. Park, C. W. Song, S. Sarkar, Y. W. Jun, Y. J. Reo, M. Dai and K. H. Ahn, *Chem. Commun.*, 2020, **56**, 7025–7028.
86 K. Hara, T. Sato, R. Katoh, A. Furube, Y. Ohga, A. Shinpo, S. Suga, K. Sayama, H. Sugihara and H. Arakawa, *J. Phys. Chem. B*, 2002, **107**, 597–606.
87 É. Torres, S. Sequeira, P. Parreira, P. Mendes, T. Silva, K. Lobato and M. J. Brites, *J. Photochem. Photobiol., A*, 2015, **310**, 1–8.
88 L. Han, R. Kang, X. Zu, Y. Cui and J. Gao, *Photochem. Photobiol. Sci.*, 2015, **14**, 2046–2053.
89 K. C. Avhad, D. S. Patil, Y. K. Gawale, S. Chitrambalam, M. C. Sreenath, I. H. Joe and N. Sekar, *ChemistrySelect*, 2018, **3**, 4393–4405.
90 K. D. Seo, I. T. Choi, Y. G. Park, S. Kang, J. Y. Lee and H. K. Kim, *Dyes Pigm.*, 2012, **94**, 469–474.
91 H. Feng, R. Li, Y. Song, X. Li and B. Liu, *J. Power Sources*, 2017, **345**, 59–66.
92 C. W. Song, U. Tamima, Y. J. Reo, M. Dai, S. Sarkar and K. H. Ahn, *Dyes Pigm.*, 2019, **171**, 107718.
93 N. Jiang, J. Fan, F. Xu, X. Peng, H. Mu, J. Wang and X. Xiong, *Angew. Chem., Int. Ed. Engl.*, 2015, **54**, 2510–2514.
94 P. S. Deore and R. A. Manderville, *Analyst*, 2020, **145**, 1288–1293.
95 P. S. Deore, D. S. Coman and R. A. Manderville, *Chem. Commun.*, 2019, **55**, 3540–3543.
96 N. Narayanaswamy, M. Kumar, S. Das, R. Sharma, P. K. Samanta, S. K. Pati, S. K. Dhar, T. K. Kundu and T. Govindaraju, *Sci. Rep.*, 2014, **4**, 6476.
97 A. Eordogh, J. Steinmeyer, K. Peewasan, U. Schepers, H. A. Wagenknecht and P. Kele, *Bioconjugate Chem.*, 2016, **27**, 457–464.
98 J. W. Yan, Y. G. Tian, J. H. Tan and Z. S. Huang, *Analyst*, 2015, **140**, 7146–7149.
99 P. Jana, M. Radhakrishna, S. Khatua and S. Kanvah, *Phys. Chem. Chem. Phys.*, 2018, **20**, 13263–13270.
100 S. K. Lanke and N. Sekar, *J. Fluoresc.*, 2016, **26**, 497–511.
101 X. D. Liu, Y. Xu, R. Sun, Y. J. Xu, J. M. Lu and J. F. Ge, *Analyst*, 2013, **138**, 6542–6550.
102 S. Zhu, W. Lin and L. Yuan, *Dyes Pigm.*, 2013, **99**, 465–471.
103 L. Yuan, W. Lin and J. Song, *Chem. Commun.*, 2010, **46**, 7930–7932.
104 F. Dubar, C. Slomianny, J. Khalife, D. Dive, H. Kalamou, Y. Guerardel, P. Grellier and C. Biot, *Angew. Chem., Int. Ed. Engl.*, 2013, **52**, 7690–7693.
105 Y. Q. Sun, J. Liu, J. Zhang, T. Yang and W. Guo, *Chem. Commun.*, 2013, **49**, 2637–2639.
106 Y. Venkatesh, K. S. Kiran, S. S. Shah, A. Chaudhuri, S. Dey and N. D. P. Singh, *Org. Biomol. Chem.*, 2019, **17**, 2640–2645.
107 K. A. Pardeshi, G. Ravikumar and H. Chakrapani, *Org. Lett.*, 2018, **20**, 4–7.
108 T. Zhang, C. Yin, Y. Zhang, J. Chao, G. Wen and F. Huo, *Spectrochim. Acta, Part A*, 2020, **234**, 118253.
109 W. Xu, C. L. Teoh, J. Peng, D. Su, L. Yuan and Y. T. Chang, *Biomaterials*, 2015, **56**, 1–9.
110 T. Zhang, L. Li, F. Huo, W. Zhang, J. Chao and C. Yin, *Sens. Actuators, B*, 2021, **342**, 130041.
111 J. Liu, Y.-Q. Sun, H. Zhang, Y. Huo, Y. Shi, H. Shi and W. Guo, *RSC Adv.*, 2014, **4**, 64542–64550.
112 X. Lv, J. Liu, Y. Liu, Y. Zhao, Y. Q. Sun, P. Wang and W. Guo, *Chem. Commun.*, 2011, **47**, 12843–12845.
113 M.-J. Peng, Y. Guo, X.-F. Yang, F. Suzenet, J. Li, C.-W. Li and Y.-W. Duan, *RSC Adv.*, 2014, **4**, 19077–19085.
114 H. Li, Z. Wen, L. Jin, Y. Kan and B. Yin, *Chem. Commun.*, 2012, **48**, 11659–11661.
115 Z. Yang, Z. Liu, Y. Chen, X. Wang, W. He and Y. Lu, *Org. Biomol. Chem.*, 2012, **10**, 5073–5076.
116 C. T. Yang, Y. Wang, E. Marutani, T. Ida, X. Ni, S. Xu, W. Chen, H. Zhang, T. Akaike, F. Ichinose and M. Xian, *Angew. Chem., Int. Ed. Engl.*, 2019, **58**, 10898–10902.
117 J. Li, Y. Cui, C. Bi, S. Feng, F. Yu, E. Yuan, S. Xu, Z. Hu, Q. Sun, D. Wei and J. Yoon, *Anal. Chem.*, 2019, **91**, 7360–7365.
118 H. Fujioka, S. N. Uno, M. Kamiya, R. Kojima, K. Johnsson and Y. Urano, *Chem. Commun.*, 2020, **56**, 5617–5620.
119 D. Zhu, X. Yan, A. Ren, W. Xie and Z. Duan, *Anal. Chim. Acta*, 2019, **1058**, 136–145.
120 X. Wu, L. Zeng, B. Q. Chen, M. Zhang, J. Rodrigues, R. Sheng and G. M. Bao, *J. Mater. Chem. B*, 2019, **7**, 5775–5781.
121 S. Singha, D. Kim, B. Roy, S. Sambasivan, H. Moon, A. S. Rao, J. Y. Kim, T. Joo, J. W. Park, Y. M. Rhee, T. Wang, K. H. Kim, Y. H. Shin, J. Jung and K. H. Ahn, *Chem. Sci.*, 2015, **6**, 4335–4342.
122 Z. Zhan, R. Liu, L. Chai, Y. Dai and Y. Lv, *Anal. Chem.*, 2019, **91**, 11461–11466.
123 H. Huang, W. Liu, X. J. Liu, Y. Q. Kuang and J. H. Jiang, *Talanta*, 2017, **168**, 203–209.
124 Y. J. Reo, S. Sarkar, M. Dai, Y. J. Yang and K. H. Ahn, *ACS Appl. Bio Mater.*, 2021, **4**, 2089–2096.
125 Y. J. Yang, M. Dai and K. H. Ahn, *ACS Sens.*, 2023, **8**(7), 2791–2798.

126 Z. Yu, W. Huang, S. Xu and S. Ke, *Microchem. J.*, 2021, **164**, 106009.
127 L. Nie, C. Gao, T. Shen, J. Jing, S. Zhang and X. Zhang, *Anal. Chem.*, 2019, **91**, 4451–4456.
128 J. Zhou, C. Yu, Z. Li, P. Peng, D. Zhang, X. Han, H. Tang, Q. Wu, L. Li and W. Huang, *Anal. Methods*, 2019, **11**, 1312–1316.
129 Y. Wang, X. Han, X. Zhang, L. Zhang and L. Chen, *Analyst*, 2020, **145**, 1389–1395.
130 Y. J. Reo, M. Dai, Y. J. Yang and K. H. Ahn, *Anal. Chem.*, 2020, **92**, 12678–12685.
131 Y. J. Kim, S. J. Park, C. S. Lim, D. J. Lee, C. K. Noh, K. Lee, S. J. Shin and H. M. Kim, *Anal. Chem.*, 2019, **91**, 9246–9250.
132 L. Yuan, W. Lin, Y. Yang and H. Chen, *J. Am. Chem. Soc.*, 2012, **134**, 1200–1211.
133 L. Yuan, W. Lin, S. Zhao, W. Gao, B. Chen, L. He and S. Zhu, *J. Am. Chem. Soc.*, 2012, **134**, 13510–13513.
134 H. Chen, B. Dong, Y. Tang and W. Lin, *Acc. Chem. Res.*, 2017, **50**, 1410–1422.
135 Z. Zeng, S. S. Liew, X. Wei and K. Pu, *Angew. Chem., Int. Ed. Engl.*, 2021, **60**, 26454–26475.
136 Y. Wen, N. Jing, F. Huo and C. Yin, *Analyst*, 2021, **146**, 7450–7463.
137 M. E. Jun, B. Roy and K. H. Ahn, *Chem. Commun.*, 2011, **47**, 7583–7601.
138 S. Singha, Y. W. Jun, S. Sarkar and K. H. Ahn, *Acc. Chem. Res.*, 2019, **52**, 2571–2581.
139 H. H. Han, H. Tian, Y. Zang, A. C. Sedgwick, J. Li, J. L. Sessler, X. P. He and T. D. James, *Chem. Soc. Rev.*, 2021, **50**, 9391–9429.

